Charles University in Prague

Faculty of Science

Department of Physiology

CLUSTER ANALYSIS OF ELECTROPHYSIOLOGICAL DATA

Bc. Stanislav Kocanda

Thesis supervisor: MUDr. et Mgr. Daniel Klement, Ph.D.

Diploma thesis

Prague 2010

Statement

I hereby declare that this diploma thesis is completely my own work and that I used only the cited sources.

Bc. Stanislav Kocanda

Acknowledgement

Here I would like to especially thank to my thesis supervisor MUDr. et Mgr. Daniel Klement, Ph.D. for teaching me the experimental methods and for his priceless help and support during the experiments as well as during the completion of this thesis.

Contents

Annotation

The thesis discusses different approaches used to extract activity of individual hippocampal neurons from multiunit recordings. It presents and compares different algorithms which have been used for this purpose. Experiments are made with intention to test the effect of MK-801 (disocilpine) in anesthetized rats and results are analyzed using described algorithms and methods.

Keywords

Anotace

Diplomová práce se zabývá různými přístupy používanými k získávání aktivity jednotlivých hipokampálních neuronů z multineuronálních nahrávek. Uvádí a srovnává různé algoritmy používané pro tento účel. Experimenty byly prováděny s úmyslem ověřit vliv podání MK-801 (dizocilpin) na neuronální aktivitu v hipokampu u anestetizovaných potkanů. Výsledky jsou analyzovány s využitím popsaných algoritmů a metod.

Klíčová slova

Shluková analýza, elektrofyziologie, extracelulární nahrávání, jednotková aktivita, hipokampus, mk-801, schizofrenie

Foreword

Electrophysiology studies the electrical properties of biological cells and tissues. In neuroscience it is a very important approach, because the electrical processes play a key role in a function of a neural tissue.

Neural electrical activity can be traced using a current-sensitive electrode. The electrode signal is amplified, filtered and then digitalized and processed using a computer. In the case of extracellular recording the signal is generated by a number of adjacent neurons. Correct assignment of the recorded activity to the respective neurones is therefore very important. The main and most commonly used method in this classification is the *cluster analysis*.

This thesis focuses on the extracellular recording of neuronal activity, especially in hippocampus. The Introduction chapter of my thesis is divided into two sections. In the first section I focus on the physical nature of the extracellular signal generated by neuronal activity and on its recording. Special attention is given to the offline processing techniques including spike detection and cluster analysis. Commonly used methods of cluster analysis are presented and their principles are briefly explained to show the limitations of these methods.

In the second section of the Introduction chapter I describe hippocampus, which is the structure of my interest in conducted experiments. The section includes a description of anatomy and physiology of the hippocampus and special aspects of recording in this structure. The role of the NMDA receptor blockers in hippocampal neuronal activity is presented as well.

In the experimental part of the thesis I present all the steps of extracellular recordings of the neuronal activity in hippocampus. Experiments were made with primary intention of achieving adequate practice through the recording process to form a solid base for further research in the deparment. The activity of hippocampal neurones was recorded in urethane-anesthetized rats before and after the application of a low dose of the NMDA receptor blocker MK-801 (disocilpine). This drug is used for modeling schizophrenic-like behavior in animals.

Chapter 1

Introduction

1.1 Extracellular recordings of neural activity

1.1.1 Physical nature of measured data

The primary function of a neuron is processing and transmission of cellular signals. The cellular signals can occur in many different forms depending on its purpose, but the main signal form processed by the neurons are the electrical signals.

Major part of the cell's electrical activity is provided by the electrochemical dynamic of its *transmembrane potential*. Controlled changes of the transmembrane potential are the main method of signalling in the neural tissue.

Structure of neuron

Neurons can have a wide variety of shapes, according to their specific position in a neural tissue, but every neuron can be simply divided into three sections:

1. *Input section.* This part of a neuron is usually formed by so called *dendrites*, cellular extensions with many branches, forming a tree-like structure. This is where the majority of input in the neuron occurs.

2. *Integration section.* This is the part of a neuron, where all the input signals are integrated and evaluated together, according to the specific weight of each input. This integration begins already in the dendrite branches and ends up in the *soma*, the central part of a neuron. The resulting sum of all the inputs is evaluated in so-called *axon hillock* at the beginning of the output section of neuron.

3. *Output section.* This part of a neuron is commonly reffered to as an *axon*. It is a variously long cable-like projection, which can extend tens, hundreds, or even tens of thousands of times the size of the soma. The axon carries the information away from the soma and transmits it to the other neurons.

The signal input to the neuron takes place in so called *synapses*, where the output section of one neuron called *presynaptic membrane* adjoins the *postsynaptic membrane*, the input section of the other neuron . The signal between the two neurons is transmitted depending on the synapse type. The most common are the chemical synapses, where the incoming signal triggers a release of a specific chemical called *neurotransmitter* from the presynaptic membrane. The neurotransmitter diffuses through the *synaptic gap,* binds to the receptors on the *postsynaptic membrane* and triggers the corresponding response.

Transmembrane potential

The transmembrane potential is defined as a difference of electric potentials between the two sides of a semipermeable *cytoplasmatic membrane*. This difference is caused by the *electrochemical gradient* of *ions*, which is induced by the semipermeability of the membrane, where the most of the substances and especially the charged substances cannot pass through the membrane freely. Therefore if there is a difference of charge concentration inside and outside the cell, a non-zero transmembrane potential occurs.

If the cytoplasmatic membrane were surrounded by the solution of one ion only, the resting potential would be equal to that ion's *equilibrium potential*. Equilibrium potential is defined as a *voltage* at which the distribution across the membrane of particular ion is in *equilibrium*. This means that the potential exactly matches (resists) the diffusive tendency of the ion, such that the net current of the ion across the membrane is zero and unchanging. The equilibrium potential of a particular ion is designated by the notation E_{ion} (i.e. for potassium the equilibrium potential $E_K = -80mV$, for sodium, $E_{Na} = +60mV$).

Equilibrium potential depends on the ion concentrations on both sides of the membrane as shows the *Nernst equation*:

$$E_{ion} = \frac{RT}{zF} \ln \frac{[ion_{out}]}{[ion_{in}]}$$

where R is the universal gas constant ($R = 8.314K^{-1}.mol^{-1}$), T is the absolute temperature in Kelvines, z is the ion valence, F is Faraday constant ($F = 9.649x10^4 C.mol^{-1}$) and $[ion_{out}]/[ion_{in}]$ are the concentrations of the ion on respective sides of the membrane.

Ion	Intracelullar [mmol/l]	Extracelullar [mmol/l]
Na^+	$5 - 15$	145
K^+	140	5
Mg^{2+}	0.5	$1 - 2$
Ca^{2+}	10^{-4}	$1 - 2$
H^+	7×10^{-5} (pH 7.2)	4×10^{-5} (pH 7.4)
Cl^-	$5 - 15$	110

Table 1.1: Ion concentrations inside and outside a typical mammalian cell. (Alberts et al., 2002)

Cytoplasmatic membrane is differently permeable for many ions, each of which contributes to the resting potential. Commonly three main ions form the

most of the resting potential and their contribution can be mathematically described using the *Goldman-Hodgkin-Katz equation*:

$$E_m = \frac{P_{K^+}}{P_{tot}} E_{K^+} + \frac{P_{Na^+}}{P_{tot}} E_{Na^+} + \frac{P_{Cl^-}}{P_{tot}} E_{Cl^-}$$

Here E_m is the membrane resting potential, E_X is the equilibrium potential for ion X, P_X is the relative permeability of ion X and P_{tot} is the total permeability of all permeant ions, in this case

$$P_{tot} = P_{K^+} + P_{Na^+} + P_{Cl^-}$$

Most of the living cells are keeping a stable value of the transmembrane potential called *resting potential*. This is achieved by the action of *ion transporters* embedded in the membrane, which maintain different ion concentrations inside and outside the cell. The concentration differences cause the inner surface of the membrane to be charged negative and the outer surface to be charged positive. The value of the resting potential in most cells lies in the range from -30 to $-90mV$. The resting concentrations of chosen ions inside and outside a typical mammalian cell are shown in table 1.1.

Signal integration

The role of a single neuron in a tissue can be simply viewed as an analog-to-digital converter. It usually summarizes a large number of electrical inputs from other neurons, and according to the resulting potential it fires an **action potential** or not.

Depending on the synapse type, the incoming singal can raise either a *depolarization* (in so called *excitatory synapses*) or a *hyperpolarization* (in so called *inhibitory synapses*) of the postsynaptic membrane potential. This potential change is initiated by opening or closing the corresponding ion channels with the activated receptors and spreads down the dendrite. This potential change propagation can be algebraically described using length and time constants.

Length constant λ is defined as

$$\lambda = \sqrt{\frac{r_m}{(r_i + r_o)}}$$

where r_m is the resistance across the membrane, r_i is the resistance inside the membrane, and r_o is the resistance outside the membrane. In calculation the

9

effects of r_o are usually negligible and therefore the equation is often simplified as

$$\lambda = \sqrt{\frac{r_m}{r_i}}$$

The resistance across the membrane is a function of the number of open ion channels and the resistance inside the membrane is generally a function of the thread width and the inner space characteristics. The length constant is used to describe the fall of the potential difference across the membrane of volume conductor according to the distance from the source

$$V(x) = V_{max}e^{-x/\lambda}$$

where $V(x)$ is the potential in the distance of x from the origin and V_{max} is defined as the maximum potential change at the origin, $V_{max} = r_m I$, where r_m is the resistance across the membrane and I is the current flow. The longer a length constant of an input is, the bigger weight the input will have along the cell.

Time constant τ is defined as

$$\tau = r_m c_m$$

where r_m is the resistance across the membrane and c_m is the capacitance of the membrane and it is a function of the properties of the lipid membrane bilayer. The time constant is used to describe the fall of the potential in time

$$V(t) = V_{max}e^{-t/\tau}$$

where $V(t)$ is the potential in time t.

Extracellular signal propagation

Electrical currents from the neuronal activity distribute in all directions from a source through the neural tissue. Electrical fields and currents in a neural tissue act according to *Maxwell's equations*. Electrical properties of a tissue can be described by **conductivity** σ which is defined as the reciprocal of electrical resistivity ρ

$$\sigma = \frac{1}{\rho}$$

and **dielectric constant** κ_r, defined as a relative static permitivity ε of the medium.

$$\kappa_r = \frac{\varepsilon}{\varepsilon_0}$$

Most of the current in a macroscopic cell suspension is expected to bypass the cells, mainly because of its linearity in the condictive sense. When tissue is linear in both dielectric and conductive senses and is subjected to an oscillating electric field of frequency f, the capacitive effect can be described by *complex conductivity:*

$$\sigma_c = \sigma(f) \left[1 + j \frac{2\pi f \varepsilon(f)}{\sigma(f)} \right]$$

Complex conductivity is a volume conductor analog of *impedance* in a normal electric circuit containing resistors and capacitors. The main consequence are the phase shifts between brain source waveforms and the corresponding potentials. But this phase shift is a different phenomenon from the phase differences observed between potentials at various locations in the brain, which are due to phase differences between many underlying current sources (Nunez and Srinivasan, 2006).

1.1.2 Data acquisition

It is possible to study the electrical activity of a neuron either by measuring its transmenbrane potential changes directly (intracellular recordings) or by measuring the potential changes in an extracellular space (extracellular recordings).

Both techniques have advantages and disadvantages. Here I will focus on the extracellular recording. As mentioned in the section above, electrical activity of a single neuron propagates through the extracellular space as the **extracellular action potential**, and it can be measured there using an extracellular electrode. The first use of microelectrodes for extracellular recording of neuronal activity was in the hippocampus by Birdsie Renshaw, Alexander Forbes and Robert Morison in 1940 (Andersen et al., 2007).

The extracellular signal is always a sumation of activity of many neurons. In the case we are able to distinguish the individual neurons in the recorded signal we can study information processing on the level of the neural networks. In addition it is possible to record the neuronal activity in freely moving animals and thus to correlate it with their behavior and stimuli presentation.

A simplified scheme of a basic set-up for the extracellular recording is shown in Figure 1.1.
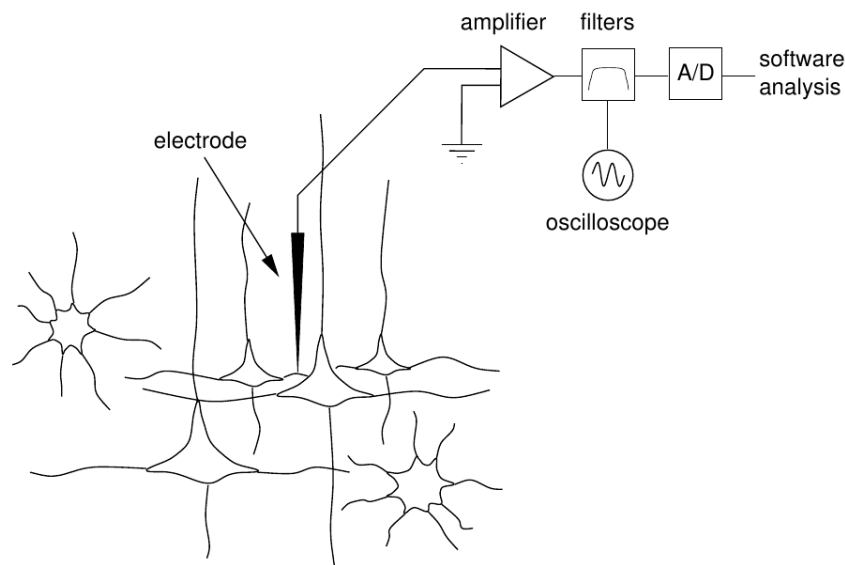

Figure 1.1: Scheme of a basic set-up for the extracellular recording. From Lewicki (1998).

Microelectrodes

The shape of the electrode affects what types of signals are measured. The larger the tip of the electrode is, the more units (neurones) are recorded, but the more difficult it is to distinguish them and vice versa (Lewicki, 1998). An ideal electrode for extracellular recording of individual unit activity has a very small volume.

The most important characteristic of the electrode is its **impedance**. It describes the electrical properties of the electrode in alternating current in the same way as **resistance** does it in direct current (in DC there is no distinction between impedance and resistance, it can be thought of as impedance with zero phase angle). The impedance affects sensitivity of the electrode and there is an effort to keep it as low as possible. Same as the resistance, impedance is a function of exposed area of the recording tip; the bigger is the diameter of an electrode, the lower is the impedance. This is in contradiction to the need for the smaller diameters electrodes suitable for the recording of individual neurones activity.

Action potentials are measured by means of extracellular glass pipettes, isolated wire electrodes with sensitive tip, or by multiple-site probes.

Glass electrodes can be used to monitor the activity of a single cell, but are not always practical in freely moving animals as these electrodes are fragile.

Wire electrodes are insulated except from the sensitive tip at the end, which represents the recording site. They provide better mechanical stability and allow for recording from one site using multiple wire electrodes in fixed bundles. The smallest bundle is made from two electrodes and was first described by McNaughton et al. (1983) as a **stereotrode**. Nowadays the most commonly used configuration is a set of four wired electrodes bundled together, referred to as a **tetrode** (O'Keefe and Recce, 1993). Using wired electrodes has numerous advantages, including easy and cheap fabrication, low-impedance recording tips, and mechanical stability. In wire electrodes the impedance can be lowered by gold plating of the tip. Their main disadvantage is that the exact configuration of the recording tips relative to the neurons can not be exactly determined (Csicsvari et al., 2003).

Factory assembled silicon probes offer great advantages over classical tetrode recording, they are substantially smaller in size and can be arranged over a longer distance. In silicon devices, the thin-film recording sites are defined lithographically (Csicsvari et al., 2003) . Any two-dimensional configuration can be achieved with proper design and can be adapted to particular brain structures and neuron types. Currently available probes can record from as many as a hundred well-separated neurons (Buzsaki, 2004). It offers precise distribution of recording sites and therefore allows for the determination of the spatial relationship of the isolated neurons. Basic problem of this approach is the price of components needed and also a certain fragility of the probe in comparison to wired electrodes.

Data preprocessing

Potential difference between given microelectrode tip and a chosen reference oscillates at values close to zero with extremes in the range of hundreds of microvolts (μV). For further data processing, this signal must be amplified (i.e. 10,000x - 50,000x). In the case of multiple channel recording, each channel must be amplified separately. Number of amplifiers available can be a limitation for the number of simultaneously recorded channels.

The electrophysiological signal is a continuous analogous signal of potential differences (see example in Figure 1.2), which has to be stored for later evaluation in a digital format. Transformation from analogous data to it's digital representation is made by an analog-to-digital converter. This device works at a given sampling frequency saving discontinuous series of voltages. This implies
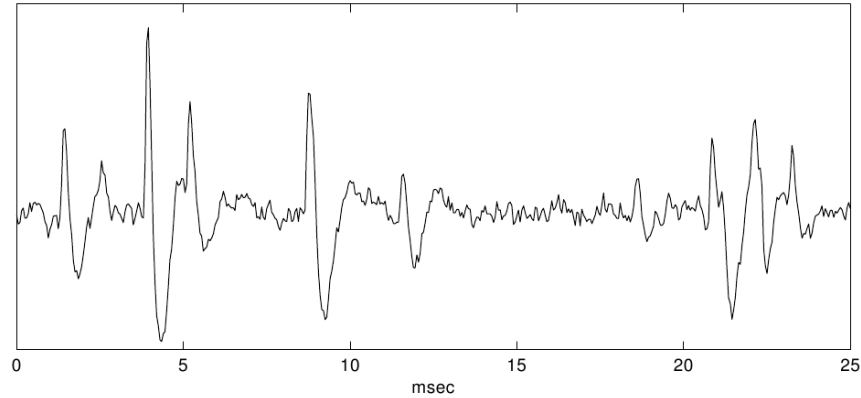
Figure 1.2: Example of extracellular record with spikes. From Lewicki (1998).

inevitable loss of information, which has non-trivial consequences, as will be shown later. The magnitude of the signal at the given sampling time is stored as a binary number, which also causes loss of precision, depending on the bit-width of the sample (usually in the range from 12 to 24 bits).

To improve the accuracy, raw data are filtered from unwanted low and high frequencies. In the case of unit activity recording filtering improves precision of the signal coding for a given bit-width.

Data storage

There are two approaches to how to save recorded data. First is to store all the data in one uninterrupted time series and do the unit activity lookup and separation later (**continous recording**). This approach provides better information about the underlying signal and noise and therefore allows for better classification of individual units. On the other side it requires large amounts of computer memory. Second approach is to detect unit activity during recording and to store only those time frames containing the expected event (**discontinuous recording**). This approach is much less storage space demanding and substantially reduces the amount of time needed for a further data processing.

1.2 Processing of the recorded data

A single extracellular electrode sums electrical activity from several neurones. Contribution of each neurone depends on its distance from the electrode's tip. To progress with data evaluation, it is essential to distinguish the individual neuronal activity in the record from each other.

Unit activity is commonly reffered to as a **spike**, short amplitude peak in the recorded potential (see Figure 1.3). This event is characteristic by its high frequency and amplitude in comparison to the noise. The crucial role in the spike sorting plays the assumption that spikes from one neurone have a waveform stable in time and spikes from different neurones have different waveforms (Buzsaki, 2004).

Figure 1.3: Example of a spike. Adapted from Lewicki (1998).

Nowadays the neuronal activity is most recorded by the means of wire tetrodes or factory-assembled probes. In both, a spike of a single neurone is recorded by several electrodes simultaneously. Each electrode records a different waveform of the spike depending on its position with respect to the neurone and therefore allows for much more precise spike sorting.

Data analysis steps

In general, the analysis consist of the following steps. These steps will be discussed in detail later:

1. **Spike detection**. In this step, individual spikes are extracted from the underlying data.

2. **Spike parametrization**. Here each spike is represented by a set of its characteristic features (feature vector).

3. **Cluster analysis**. Feature vectors are then classified and sorted using cluster analysis algorithms.

4. **Cluster quality assessment**. The quality of clusters produced by chosen cluster analysis algorithm is evaluated and only clusters with a sufficient quality are used for further analysis.

Graphical overview of the basic steps is shown in Figure 1.4.
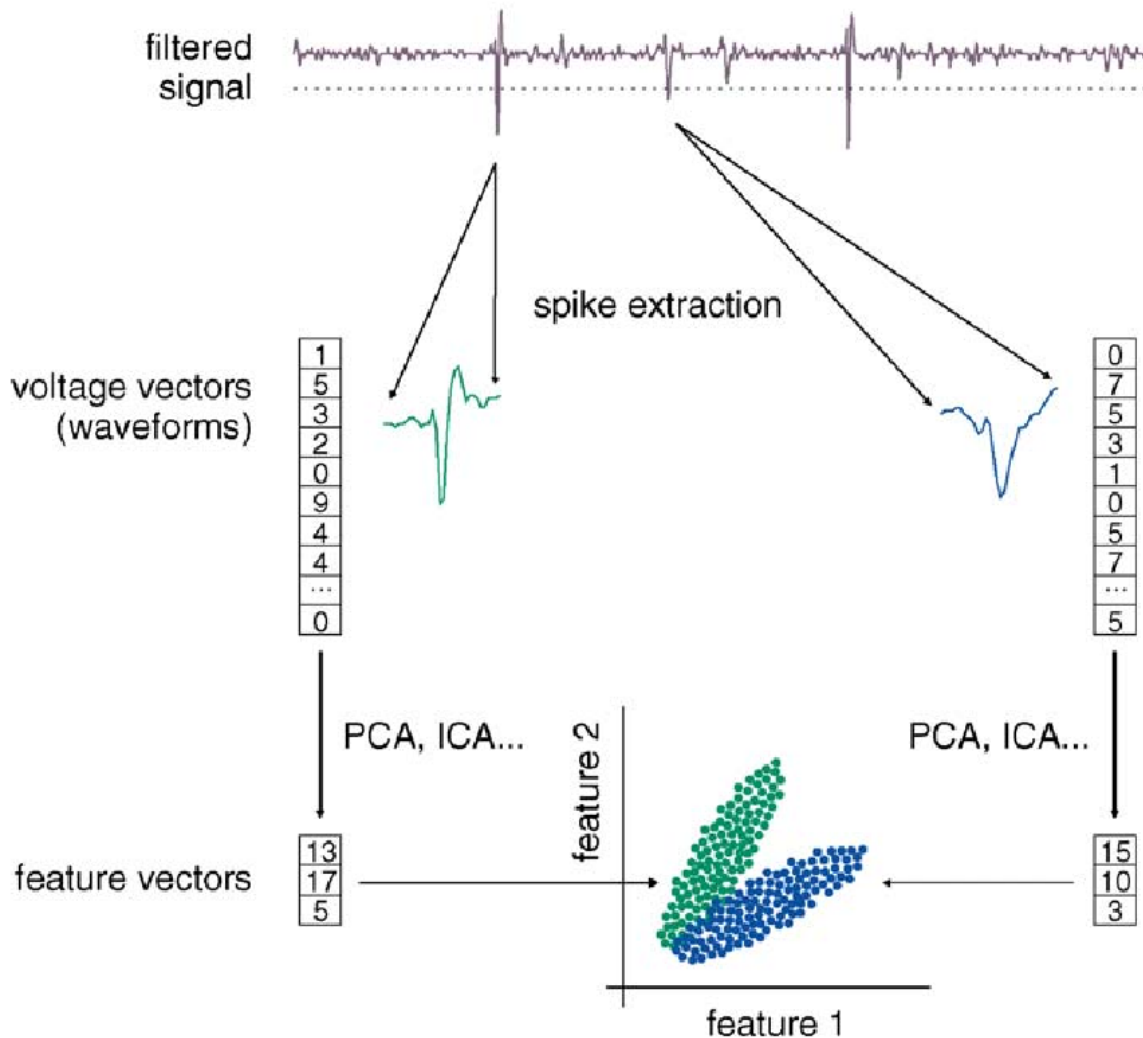
Figure 1.4: Overview of electrophysiological data processing. From Hazan et al. (2006).

1.2.1 Spike detection

The recorded data represent noise combined with spikes from several neurones. The task of the spike detection is to distinguish and isolate the individual spikes in the record.

Spike is characteristic by it's waveform. A sharp peak in the record highly above the noise level. Therefore it is usually detected by crossing a given thresh-

old. In discontinuous recordings it is the main approach because of its fast evaluation (Lewicki, 1998). Choosing a proper threshold value is a key part of the experiment especially in discontinuous recordings. If the threshold is set too high, lots of spikes are lost, if the threshold is set too low the record contains an unwanted fraction of fake noise spikes that crossed the threshold because of random sumation of extracellular potentials.

In continuous records it is possible to use the threshold detection as in the discontinuous recordings, beside of it it is possible to use the energy of the signal to detect the presence of spike, because the mean energy of a spike is expected to be significantly higher than the mean energy of the underlying noise. Energy from a given time frame is then compared with mean energy of the whole data and if the energy difference crosses a given threshold value, it is marked as a spike.

After spikes are detected, they are usually isolated and separated from the rest of the record to reduce the total amount of processed data. In all continuous or discontinuous records the time frame saved is always started several samples before the point of detection to keep the very beginning of the spike and its width covers the expected length of the spike.

One of the basic problems of spike isolation is possible presence of overlapping spikes. Frequency of overlaps depends on the firing rates of the units involved. The percentage of missed spikes is defined by the probability that the peak of the isolated spike will occur during the negative phase of the preceeding spike. It can be quantified as $100rd/1000[\%]$, where r is the firing rate in hertz and d is the duration of the negative phase in milliseconds (Lewicki, 1998). Thus if the preceeding neurone is firing at 20 Hz and the duration of the negative phase is approximately 0.5 ms, then approximately 1 % of the spikes will be missed.

Another source of error is simultaneous firing of two or more neurones with their spikes not reaching the threshold. Sumation of the spikes can cross the threshold and be recorded. In this case, if two independent neurons have rates $r1$ and $r2$, then their spikes will sum to cross threshold at a frequency of approximately $r1r2d/1000$, where d is the spike width in milliseconds (Lewicki, 1998). If the two background neurons have firing rates of 20 Hz and the spike width is 0.25 ms, then they will generate false positives at a rate of 0.1 Hz.

Introduced equations will typically underestimate the frequency of missed or overlapping events because of a possibly high correlation of firing patterns in adjacent neurons.

1.2.2   Spike parametrisation

Each spike is represented by a set of values. The values encode a shape of the spike. Number of the values depends on the time frame width and sampling frequency. Thus the spike can be formally viewed as an n-dimensional vector, where n is the number of values. The dimension is usually 32 or 64 samples. In the case of multi-channel electrodes (i.e. tetrodes) the number of dimensions increases, for tetrodes usually 128 or 256 dimensions for a single spike.

The task of spike classification therefore involves evaluation of similarities and dissimilarities in a high-dimensional vector space. It is very computationally demanding and slow. To reduce the dimension of the vector space, each spike is represented by a set of suitable parameters, which form a new vector with a much lower dimension.

Commonly used features include measures of the shape, like spike height and width or peak-to-valley amplitude. These features are very easy to calculate and are therefore used mainly in the conditions with restricted computer resources. Another widely used approach is the use of **principal component analysis**. (Lewicki, 1998)

The idea behind the principal component analysis (PCA) is to find a new basis of the vector space. As a result most of the data variability is represented along the first dimension of the new basis, the most of the remaining variability along the second dimension and so on. Therefore it is usually sufficient to represent the data using only a few first elements of the transformed vectors, mostly three, reffered to as PC_1, PC_2 and PC_3 (PC standing for Principal Component). (Lewicki, 1998)

Waveform interpolation

To achieve better performance in spike classification, signal is sometimes upsampled by interpolation using *discrete convolution* with an appropriate reconstruction function, i.e. sinc function:

$$s(t) = \sum_{n=-\infty}^{n=\infty} s(n)h(t-n)$$

where $s(t)$ is the reconstructed waveform voltage at time t, $s(n)$ is the raw voltage waveform sampled at time intervals $n = 1, 2, 3, ...$ and $h(t)$ is the sinc reconstruction function:

$$h(t) = \frac{\sin \pi t}{\pi t}$$

This interpolation allows for better waveform estimate and more precise feature assesment. Other interpolation methods can be also used, bud only Fourier-based techniques have a solid teoretical grounding. Alternative methods like cosine, Gaussian, polynomial or cubic spline interpolation are useful for display purposes but do not give the best results (Blanche and Swindale, 2006).
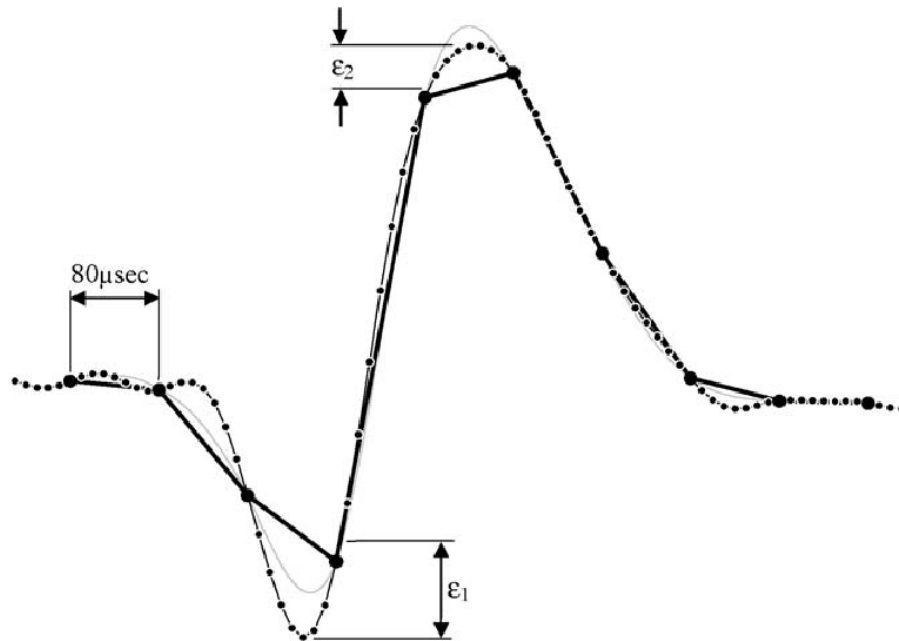

Figure 1.5: Example of an interpolated spike sampled at the Nyquist rate (12.5 kHz, large dots) and the original waveform (sampled at 100 kHz, fine black line). Spike amplitudes are underestimated by ε_1 and ε_2. The cubic spline interpolated waveform (fine grey line) is shown for comparison. From Blanche and Swindale (2006).

Information carried by spike

As shown in Gold et al. (2006), extracellular action potential carries not only the information about electrode position in relation to the firing cell, but it is also modified by composition of ionic currents in different cells. It has been shown that each cell's dendritic morphology had very little impact on extracellular action potential waveform.

Henze et al. (2000) reported several parameters of an intrucellularly recorded action potentials that can be deduced from extracellularly recorded spike waveforms. One is the width of the intracellularly recorded action potential, which is defined precisely by distinct points on the extracellular spike. Another parameters are the amplitude changes of the intracellularly recorded action potential, which are reflected by changes in the amplitude of the initial negative phase of

19

the extracellular action potential. These amplitude changes are dependent on the state of the network.

1.2.3 Cluster analysis

Cluster analysis is a method of grouping objects from a data set according to their similarities and dissimilarities. Objects in a cluster should be similar to one another and different from objects in another cluster.

Types of clusterings

A set of clusters is often called **clustering** and we can distinguish several types of clusterings (from Tan et al., 2005):

- *Hierarchical* versus *Partitional clustering*: A partitional clustering is simply a division of the dataset into non-overlapping subsets (clusters); hierarchical (or *nested*) clustering allows existence of subclusters and clusters here are organized in a tree, where each node (cluster) in a tree (except for the leaf nodes) is the union of its subclusters.

- *Exclusive* versus *overlapping* versus *fuzzy:* Clusterings shown in Figure 1.6 are all exclusive, because they assign each object to a single cluster. There are many situations in which an object can be reasonably assigned to more than one cluster, these clusterings are reffered to as overlapping or *non-exclusive*. In fuzzy clustering every object belongs to every cluster with a membership weight in the range from 0 (absolutely doesn't belong) to 1 (absolutely belongs). In fuzzy clustering it is often imposed that the total sum of weights for each object must equal 1.

- *Complete* versus *partial:* A complete clustering assigns every object to one of the clusters, whereas in partial clustering there remain some objects unclustered. In electrophysiology it is almost always partial clustering, as there is a fraction of clusters which represent uninteresting noise.

Types of clusters

Cluster analysis tries to find useful groups of objects, where usefulness is determined by the goals of the analysis. There are several notions of a cluster that proved useful in practice (examples are shown in Figure 1.7) (from Tan et al., 2005):
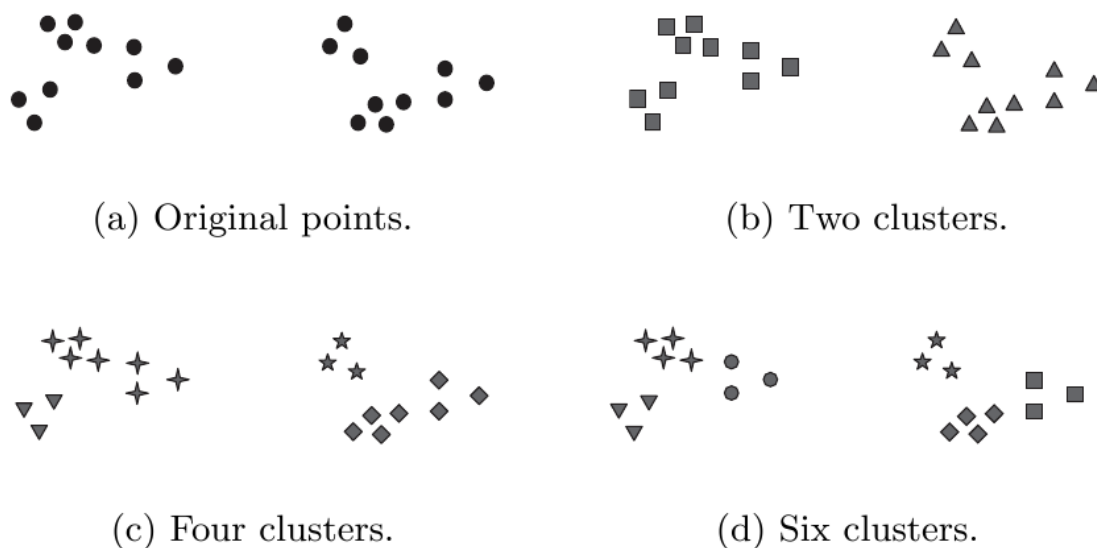
(a) Original points.

(b) Two clusters.

(c) Four clusters.

(d) Six clusters.

Figure 1.6: Different ways of clustering the same dataset. From Tan et al. (2005).

- *Well-Separated:* In well-separated clusters each object is closer (or more similar) to every other object in the cluster than to any object not in the cluster. Well-separated clusters can have any shape, but the distance between them must be larger than the distance between any two objects within a group. Therefore it is usable only when the data form natural clusters that are quite far from each other.

- *Prototype-Based:* A cluster is defined by its prototype object and it contains all the objects, that are more similar to this prototype than to prototypes from other clusters. For data with continuous attributes the prototype of a cluster is often a centroid (i.e. the average of all the points in the cluster); for categorical attributes the prototype is often a medoid (i.e. the most representative point of a cluster). These clusters are commonly reffered to as *center-based clusters.*

- *Graph-Based:* In the case of data that can be represented as a graph, where the nodes are objects and the links represent connection among objects, cluster can be defined as a *connected component* - a group of objects that have connection to one another and no connection to objects outside the cluster. Example of graph-based clusters are *contiguity-based clusters*, where two objects are connected if they are within a given distance of each other.

- *Density-Based:* A cluster is defined as a region with high density of objects,

surrounded by a region of low density.

- *Shared-Property (Conceptual Clusters):* Objects in such a cluster share some property. This definition encompasses all the above definitions, however the shared-property type include also some new types of clusters.
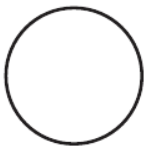
(a) Well-separated clusters. Each point is closer to all of the points in its cluster than to any point in another cluster.
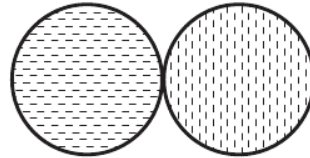
(b) Center-based clusters. Each point is closer to the center of its cluster than to the center of any other cluster.
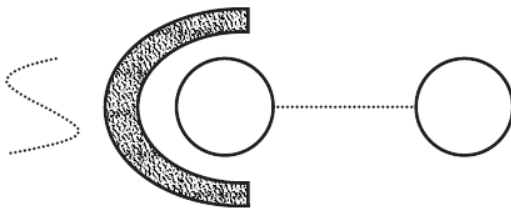
(c) Contiguity-based clusters. Each point is closer to at least one point in its cluster than to any point in another cluster.
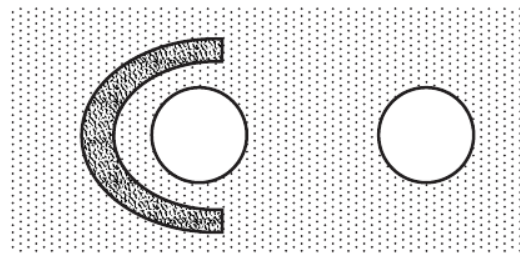
(d) Density-based clusters. Clusters are regions of high density separated by regions of low density.
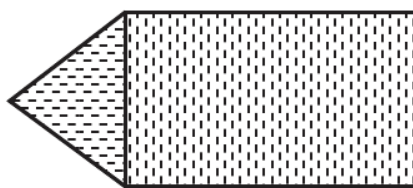
(e) Conceptual clusters. Points in a cluster share some general property that derives from the entire set of points. (Points in the intersection of the circles belong to both.)

Figure 1.7: Examples of different types of clusters. From Tan et al. (2005).

Cluster analysis in electrophysiology

In electrophysiology the cluster analysis is mainly used for classification of spikes. There is an assumption that the underlying data result from several independent classes, which are expected to represent different neurons and form different clusters. (Lewicki, 1998)

Clustering is commonly accomplished using manual clustering function in one of the available software for this purpose. There are implemented algorithms for automatic clustering in electrophysiology, nevertheless these algorithms are not reliable enough for a fully automatic data processing. They are commonly used in a semi-automatic manner, i.e. the produced results are reviewed and refined by the operator manually.

In electrophysiology it is mostly a partial clustering, because there is always a fraction of events that is likely to be a noise rather than a distinguishable spike activity. It is also exclusive clustering, because one spike is expected to be generated by one neurone only and there is no way to assign one spike to more neurones in real.

1.2.4   Manual clustering

The most basic method of cluster analysis is manual clustering. This is done using some kind of graphical interface program, which allows an operator to select two feature vector elements to create a two-dimensional scatter plot from those elements. The operator then draws polygons around a subset of spikes assigning the spikes to a common cluster. By viewing other projections, the operator can adjust and refine the cluster's boundaries. (Harris et al., 2000)

This method is highly subjective and irreproducible, as even the same experimenter does not get exactly the same results on the same data set. Nevertheless with an experienced operator the results differ only slightly and for most of the experimental settings those slight differences do not have a significant influence on the results.

There are several software solutions made solely for the purpose of manual cluster analysis of electrophysiological data, i.e. WClust, MClust**,** Klusters, Spikesort 3D and others. Here I will describe in more detail those I have been working with.

MClust

MClust is an toolbox for Matlab™(The MathWorks Inc.) being developed by A. David Redish since 1998 (Redish et al., 2010). The current version is

MClust 3.5A released on April 2008 and requires Matlab™ version 2007a or higher.

MClust loads raw waveform data, calculates chosen features from the data and displays a scatter-plot for the manual clustering. MClust is equipped with loading engine for Neuralynx data format, but a custom loading engine can be developed according to the requirements described in the documentation, so any data format can be proccessed in MClust.

Basic cluster features in MClust include *peak* (maximum height of the waveform for each channel), *energy* (waveform energy for each channel), *time*, *principal components 1, 2 and 3* (first three components of the principal component analysis). There are also additional features like *area* (area within the waveform), *valley* (maximum depth of the waveform), *peak to valley ratio*, *spike width* and others. It is possible to develop and add new features according to the requirements described in MClust documentation as well.

MClust allows the operator to view many properties of the created clusters and includes implemented algorithms for calculation of cluster quality measures, namely *Isolation distance* and *L-ratio* (see section 1.2.8 for details).

Klusters

Klusters is a standalone application available for all common platforms. It is distributed under the GNU General Public License for free as a source code and can be compiled in all common operating systems (Hazan et al., 2006). As there is no need for supportive software (as it is for Matlab in the case of MClust), the overall costs of Klusters usage are minimal.

In contrary to MClust, Klusters has its exactly defined data file structure, which is described in the documentation. Klusters does not include tools for feature calculation, feature data have to be loaded from a separate file created by another program.

1.2.5 Automatic clustering

Automatic clustering algorithms try to sort a given set of feature vectors into separate clusters. As in the electrophysiology the number of clusters (neurones) is not known, these algorithms have to estimate the proper number of clusters, that gives the best clustering results.

K-Means

One of the general clustering algorithms is *K-Means* (Tan et al., 2005). This is an iterative algorithm that basically runs in the following steps:

1. Select K points as initial centroids.

2. **repeat**

    (a) Form K clusters by assigning each point to its closest centroid.

    (b) Recompute the centroid of each cluster as a mean of the points assigned to this cluster in (a).

3. **until** Centroids do not change.

K-Means has been used in electrophysiology by Takahashi et al. (2003), but it is not widely used because it requires an estimation of the number of clusters. K-Means also fails to cluster "natural" clusters, when they have non-spherical shapes or widely different sizes or densities (Tan et al., 2005).

KlustaKwik

KlustaKwik is a program for unsupervised classification of multidimensional continuous data (Harris, 2002). KlustaKwik is based on the Classification Expectation Maximization (CEM) algorithm (Celeux and Govaert, 1992). It also uses several tricks to improve execution speed while maintaining good performance.

KlustaKwik accepts a set of feature vectors in a "feature file" input and a set of additional parameters. It produces two output files, the "cluster file" and a log file. Input file should be named according to the convention described in the documentation. The cluster file contains the number of classes chosen by the program and assignment of classes to the input vectors.

The additional parameters include *MinClusters* and *MaxClusters*, which restrict the random initial assignment. The initial number of clusters will be in the range from MinClusters to MaxClusters, but the final number may be different, since clusters can be split or deleted during the course of the algorithm. There is also the *MaxPossibleClusters* parameter, which reduces the maximal final number of created clusters. All the parameters are described in the documentation file.

BubbleClust

BubbleClust is an application developed by Peter Lipa, University of Arizona (Horton et al., 2007) and now provided by Neuralynx Inc.

BubbleClust is based on the kth-nearest neighbour algorithm (Daly et al., 2004). BubbleClust produces a decision tree that segregates events from the lowest to the highest neighbor density. It groups spikes according to the nearest-neighbor distances, clustering spikes that are close to each other.

SOMA

SOMA is an implementation of a machine learning algorithm for spike sorting described by Horton et al. (2007).

First, the algorithm estimates the number of clusters using a proposed extension to the *Kohonen method* based on the principle of self-organising maps (*Kohonen networks*). After the number is determined, spikes are assigned to the clusters according to the nodes produced in the first step, reducing misclassification using extra nodes, whose position is iteratively updated and moved towards the edge of the cluster.

1.2.6   Semi-automatic clustering

Results of the automatic algorithms are considered not to be sufficiently accurate in comparison to the manual clustering. Often used approach is to perform automated clustering using some of the algorithms and then refine the produced clusters using some of the manual clustering tools.

MClust is deployed together with KlustaKwik and BubbleClust implementations and allows for the easy results refinement. Klusters program is developed with respect to the data structure produced by KlustaKwik and it is therefore easy to combine these two.

The refinement usually includes merging of the clusters that seem to belong together according to the operator's experience and deleting clusters that are obviously formed from noise spikes.

1.2.7   Online clustering

There are two different approaches to cluster analysis. The first is to perform clustering on the whole dataset after the recording is done. This so called **offline clustering** is more common, because it allows for better feature analysis and cluster quality assessment. Another approach is to cluster data online

(**online clustering**) while recorded. This setting allows for "closed-loop" experiments, i.e. the adaptation of the experiment to the observed neural response. (Rutishauser et al., 2006)

As the online clustering needs to be performed in realtime, it must be done using some automatic clustering algorithm. Some algorithms require a learning phase, after which neurons are classified (Aksenova et al., 2003).

1.2.8 Cluster quality assessment

Cluster analysis produces a set of clusters. For further analysis it is necessary to distinguish between good clusters that are well-separated from others, and bad clusters, which are not so reliable.

In electrophysiology there is not only a need for well-separated spikes. It is also crucial that the spikes in one cluster come from one neurone. Assuming the spikes generated by a single neurone, the **inter-spike interval** should exceed the absolute refractory period, in which the neurone is not able to fire an action potential. This refractory period uses to be in the range of miliseconds (Kandel et al., 1991). Therefore if there are at least two spikes in the cluster in a shorter interval, the cluster has to be considered to represent a multi-unit activity.

In most cases, it is still a subjective judgment of human experimenter who evaluates clusters quality according to his experience. This approach is highly irreproducible and precludes comprehensive assessment of single-unit studies, and therefore there were suggested metrics that evaluate the cluster quality.

In the following text I will use $\mathcal{C}$ as a symbol for a set of spikes in a cluster and $n_{\mathcal{C}}$ as a symbol for the cardinality of $\mathcal{C}$: $n_{\mathcal{C}} = |\mathcal{C}|$.

Signal-to-noise ratio

Signal-to-noise ratio is usually used to define an overall quality of the recorded signal. Joshua et al. (2007) describes two ways of computing signal-to-noise ratio for a given cluster. Both methods compute the signal in the same fashion but differ in their noise definition:

The average cluster waveform of a cluster $\mathcal{C}$ (in which all the spikes were aligned by the negative peak) is defined as:

$$\boldsymbol{X}_{avg} \equiv \frac{1}{n_{\mathcal{C}}} \sum_{\boldsymbol{X} \in \mathcal{C}} \mathbf{X}$$

Signal is then quantified as the difference h between the minimum and maximum of the average spike waveform:

$$h = Max(\boldsymbol{X}_{avg}) - Min(\boldsymbol{X}_{avg})$$

Signal-to-noise ratio (SNR) is then calculated as

$$SNR = \frac{h}{Noise \times F}$$

where F is a scaling factor and $Noise$ is defined in two ways:

1. As the standard deviation of a so-called $Resid$ vector. This vector is as concatenation of all spike residuals in the cluster, where one spike residual is calculated by subtracting its waveform vector from the vector of the mean cluster waveform

2. As the standard deviation of a so-called $Prev$ vector. This vector is a concatenation of 1.5-3ms period preceeding the spike.

Joshua et al. (2007) states that signal-to-noise ratio can become problematic in some cases, especially in cases where the spike cluster actually reflects high amplitude multi-unit activity.

Isolation score

Joshua et al. (2007) describes *Isolation score* as a good alternative to the Signal-to-noise ratio. Isolation score quantifies the distance between the spike cluster and the unclustered noise spikes. Joshua et al. (2007) presents a list of general requirements for definition of a good formula for calculating quality score:

1. The score should decrease with the increasing number of spikes that should belong to the cluster, however were missed by the sorting algorithm (false negatives).

2. The score should decrease with the increasing number of noise events that were classified as spikes (false positives).

3. The score should be insensitive to the size of the extracted noise spikes.

4. The score should span an intuitive range, e.g. 0-1.

The presented score is defined as

$$IS = \frac{1}{n_{\mathcal{C}}} \sum_{\boldsymbol{X} \in \mathcal{C}} P(\mathbf{X})$$

where $P(\boldsymbol{X})$ can be viewed as a measure of probability that spike $\boldsymbol{X}$ belongs to the cluster $\mathcal{C}$. It can be viewed as a probability that event $\boldsymbol{X}$ belongs to the spike cluster. Range of IS is from 0 to 1, where score of 1 means ideal isolation with all spikes surely belonging to the cluster.

Isolation distance

Schmitzer-Torbert et al. (2005) describes *Isolation distance* as a useful cluster quality measure. It is based on calculation of *Mahalanobis distance*. Mahalanobis distance $D^2_{\boldsymbol{x},\mathcal{C}}$ of a spike $\boldsymbol{x}$ from the center of a cluster $\mathcal{C}$ is defined as

$$D^2_{\boldsymbol{x},\mathcal{C}} = (\boldsymbol{x} - \boldsymbol{\mu}_{\mathcal{C}})^T S_{\mathcal{C}}^{-1} (\boldsymbol{x} - \boldsymbol{\mu}_{\mathcal{C}})$$

where $\boldsymbol{x}$ is a feature (column) vector of the spike and $\boldsymbol{\mu}_C$ is the mean (column) vector of the values of the spikes in cluster $\mathcal{C}$. $S_{\mathcal{C}}$ is a covariance matrix of the spikes in the cluster $\mathcal{C}$. Mahalanobis distance allows for the measurement of the distance between objects in a high-dimensional space where there is a correlation between dimensions. This can be observed for example in peaks of spikes on different electrodes. In this case, the cluster has an elongated shape, reflecting the correlation between the peaks.

Isolation distance is defined as the $D^2_{\boldsymbol{x},\mathcal{C}}$ value of the $n_{\mathcal{C}}^{th}$ closest noise spike. It is the radius of the smallest ellipsoid from the cluster center containing all the cluster spikes and equal number of noise spikes. Isolation distance is not defined in the case where the number of cluster spikes is greater than the number of noise spikes.

L-ratio

If the cluster $\mathcal{C}$ has a multivariate normal (Gaussian) distribution, then the Mahalanobis distance $D^2_{\mathcal{C}}$ (see above) will distribute as χ^2_{df} with the number of degrees of freedom equal to the feature space dimension. A scalar L is defined as:

$$L(\mathcal{C}) = \sum_{\boldsymbol{x} \notin \mathcal{C}} 1 - \mathbf{CDF}_{\chi^2_{df}}(D^2_{\boldsymbol{x},\mathcal{C}})$$

where $CDF_{\chi^2_{df}}$ is the cumulative distribution function of the χ^2_{df}. A low value of L indicates that the cluster is well separated, whereas a high value indicates that it is likely to include spikes that are not part of the cluster and exclude spikes that should be in the cluster. L_{ratio} is defined as L divided by the total number of spikes in the cluster:

$$L_{ratio}(\mathcal{C}) = \frac{L(\mathcal{C})}{n_{\mathcal{C}}}$$

Using L_{ratio} instead of L allows larger clusters to be more tolerant to contamination, but in situations where even small amounts of misclustered spikes can bias the results, L can be more appropriate quality measure (Schmitzer-Torbert et al., 2005).

Problems affecting cluster quality

There are several issues that can influence the cluster quality and usefulness of cluster analysis (from Lewicki, 1998):

1. *Burst-firing neurons:* As mentioned above, the key assumption in such an analysis is that spike shapes originating from one neurone are stable and do not change in time. This is not always true. In the case of a bursting cell (typical for e.g. complex spike cells), the consecutive spikes tend to have decreasing amplitudes. There are clustering techniques such as multivariate Gaussian clustering, that can classify burst accurately if the attenuation is not too large.

2. *Electrode drift:* As a response to pressure from the advancement of the electrode, the neural tissue relaxes and neurones drift slowly to a different position in respect to the recording tip. This usually results in a gradual change of spike shapes. The problem can be solved either using the same approach as in bursts or by splitting the data into a short time interval, in which chosen features remain relatively constant, and to cluster each interval separately.

3. *Non-stationary background noise:* If there is a fluctuating background noise level, many more misclassifications will occur during high levels of noise. This can be solved using a variable estimation of the classification reliability depending on the background noise level, but it is rarely used because of the complexity of time-varying noise model implementation.

4. *Spike alignment:* In a small region of neural tissue, neurones often fire in a synchronous pattern and show an alignment, which can sometimes result in an overlapping. Typically spikes are aligned with respect to the amplitude peak.

1.3 Hippocampus

Hippocampus is one of the most intensively studied anatomical parts in the rat's brain. Its cellular structure is well known and it is the main subject of extracelular neuronal activity recordings. The name hippocampus comes from its appearance resembling a seahorse (fish of the genus hippocampus).

Hippocampus plays an important role in formation of declarative memory across species (Eichenbaum and Otto, 1992) . In rats, hippocampus has proved its importance in spatial navigation (O'Keefe and Nadel, 1978; Morris et al., 1982) and place recognition (Klement et al., 2005).

1.3.1 Anatomy

Hippocampus is a curved sausage-shaped pair structure, situated at the base of medial temporal lobes in forebrain (see Figure 1.8). In rats, hippocampus occupies a large portion of the forebrain. Hippocampus is a part of a **hippocampal formation**. It includes the **dentate gyrus** (fascia dentata), the **hippocampus proper** (Cornu Ammonis) and the subiculum (Fix, 2008). Some authors include also presubiculum, parasubiculum and ethorinal cortex in the hippocampal formation (Andersen et al., 2007).

Dentate gyrus and the hippocampus proper form two U-shaped interlocking sectors. Dentate gyrus is divided into internal (buried) and external (exposed) blade, hippocampus proper is further divided into four fields, CA1-4, CA standing for Cornu Amonnis.(O'Keefe and Nadel, 1978).

Hippocampus in mammals is a three layered (neocortex consists of six layers). It consists of principal cells and interneurones.

With the exception of CA4, the basic pattern in all fields of the hippocampus is the same: an ordered sheet of principal neurones whose cell bodies are all packed together in one layer (granular layer in dentate gyrus and pyramidal layer in Cornu Ammonis).

Hippocampus is a part of so-called **limbic system** together with cingulate cortex, olfactory cortex, and amygdala (Andersen et al., 2007). These regions are highly interconnected and do interact with one another.

Cell types

The principal neurones in the hippocampus proper are **pyramidal cells**, excitatory neurones with the triangular shaped soma (cell body), after which the
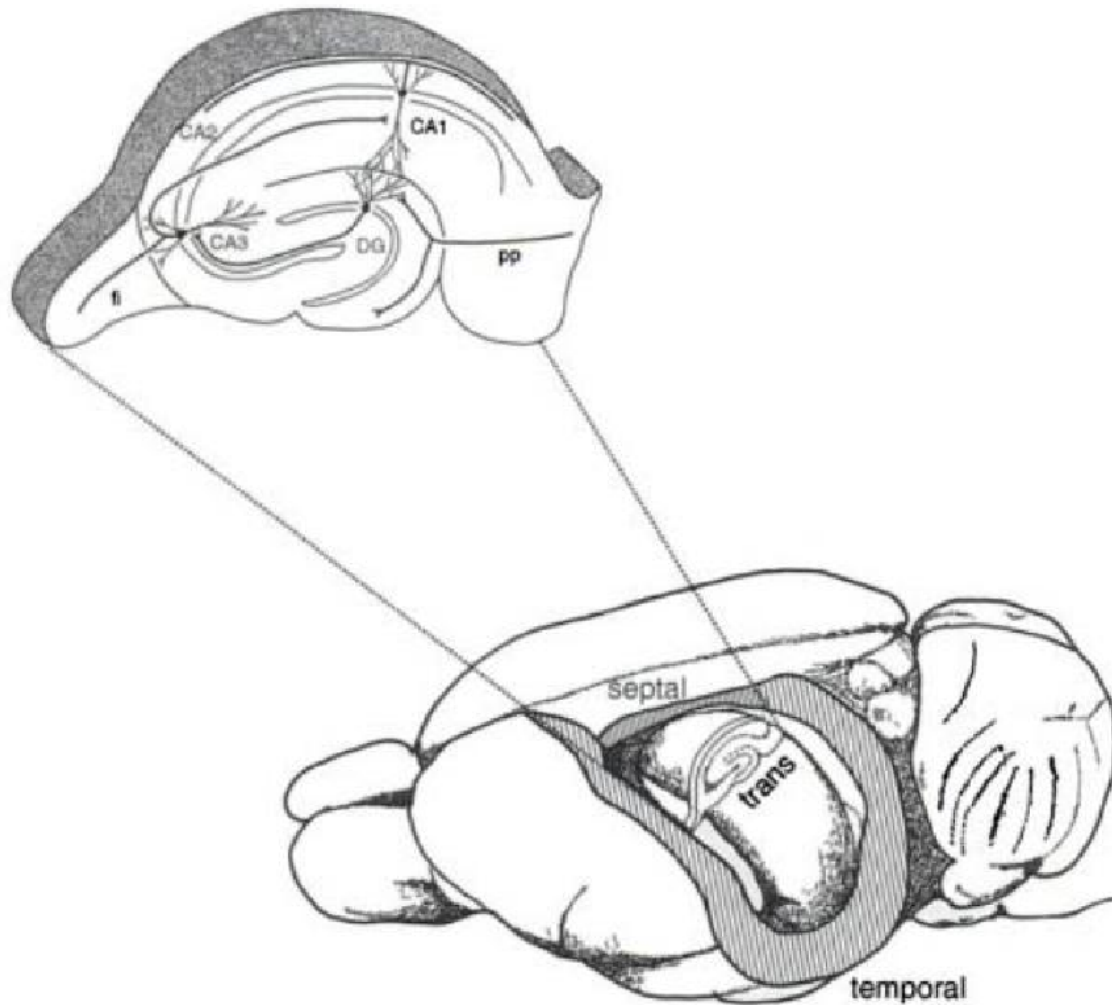
Figure 1.8: Line drawing of the rat brain. It shows the septotemporal and transverse axes of the hippocampal formation. From Andersen et al. (2007)

neurone is named. Pyramidal cell have a single axon, a large apical dendrite and multiple basal dendrites.

Principal cell type in dentate gyrus are **granule cells** which in comparison with pyramidal cells have only apical dendrites.

Most abundant (Freund and Buzsaki, 1996) interneurones in hippocampus are so called **basket cells**. Their axons ascend through the cell-body layer, moving orthogonally to the dendrites of the pyramidal or granule cells, giving off numerous descending collaterals which end in basket-like plexuses around the cell bodies.

Other **interneurones** (e.g. the stellate and fusiform cells of Cajal) send their axons into the apical dendritic layer to make contact with the distal dendrites of

the pyramids and granules. There is physiological evidence that some of the interneurones exert a widespread inhibitory control over the pyramidal and granule cells. (McBain and Fisahn, 2001; Andersen et al., 2007)

Layering

Dentate gyrus has three layers starting from superficial to deep layers:

1. The *granule* layer containing densely packed cell bodies of the granule cells;

2. the *molecular* layer formed by the intertwinning apical dendrites of the granule cells and their afferents;

3. the *polymorph* layer in the hilus of dentate gyrus merging with the CA4 field, which contains the initial segments of the granule-cells axons as they gather together to form the mossy fibre bundle.

Hippocampus proper is basicaly a three-layered structure just like the dentate gyrus, but it has been divided into seven distinct layers:

1. The *alveus*, most superficial layer containing axons from pyramidal cells;

2. the *stratum oriens*, next layer below alveus containing basal dendrites of the pyramidal cells and also basket cells, as well as afferents from the septum;

3. the *stratum pyramidale* containing cell bodies of pyramidal cells;

4. the *stratum lucidum*;

5. the *stratum radiatum* containing septal and commisural fibres. It also contains Schaffer collateral fibers which are the projection forward from CA3 to CA1.

6. the *stratum lacunosum*, a thin stratum that also contains Schaffer collateral fibers and in addition perforant path fibers from the superficial layers of entorhinal cortex. Due to its small size, it is often grouped together with stratum moleculare into a single stratum called stratum lacunosum-moleculare;

7. the *stratum moleculare.*

(Andersen et al., 2007)

Connections

The cells of the hippocampus receive afferents from several sources (O'Keefe and Nadel, 1978; Shepherd, 2004):

1. Intrinsic afferents from cells of the same field. There are two types of interactions between pyramidal cells within the same CA field: a direct excitatory one and an indirect inhibitory one.

2. Intrinsic afferents from other sectors. The major interconnections between the three sectors are, primarily unidirectional, starting from the dentate gyrus, coursing through the CA3 field, and ending in CA1. Unmyelinated axons of dentate gyrus granule cells project along the **mossy fiber pathway** to the CA3 region. These axons emerge from the basal portions of the granule cells and pass through the hilus of the dentate gyrus before entering the stratum lucidum of CA3. The pathway was named so by *Ramon y Cajal* because the axons display varicosities all along their lengths, giving them a "mossy" appearance. Mossy fibers form multiple synapses with the elaborate dendritic spines of CA3 pyramidal cells in stratum lucidum. So called **Schaffer collaterals** are axons of CA3 pyramidal cells which project to CA1.

3. Commissural afferents from the opposite hippocampus. Extensive connections exist between the two hippocampi crossing the midline in the ventral and dorsal hippocampal commissures.

4. Extrinsic afferents from outside the hippocampus:

   (a) From cortical regions. The dentate gyrus receives its major input from enthorinal cortex through so called **perforant path**. The projection to the dentate gyrus arises mainly from layer II of the enthorinal cortex. A minor component also comes from the deep layers of the enthorinal cortex.

   (b) From subcortical regions. Subcortical inputs to the dentate gyrus originate mainly in the septal nuclei, supramamillary region of the posterior hypothalamus and several nuclei in the brainstem, especially the locus coeruleus and raphe nuclei.
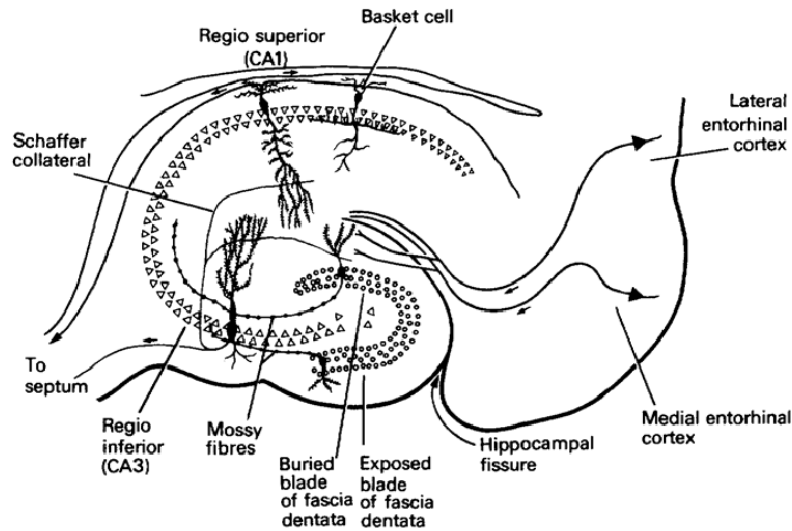
Figure 1.9: Schematic diagram of the intra-hippocampal connections. Horizontal section through the right hippocampus. From O'Keefe and Nadel (1978).

1.3.2 Physiology

Hippocampal EEG

Physiological activity of hippocampus can be easily studied using EEG recordings. Hippocampus shows three basic types of overall EEG activity:

1. A slow sinusoidal rhythm which normally ranges from 3 to 7 Hz in rabbit, dog, and cat, and 6 to 10 Hz in the rat and gerbil. This rhythm has been called **theta**, or rhythmical slow activity.

2. Large irregular amplitude waves in which the dominant frequency is slower than in theta and which, with some electrode placements, contain so called **sharp waves** of 50-100 ms duration.

3. Small irregular amplitude, desynchronized, high-frequency pattern which rarely lasts for more than a second or two in the rat, but can be more sustained in rabbit and cat.

The hippocampus contains neural circuitry which tends to oscillate at the frequencies of hippocampal theta. According to depth-mapping studies of hippocampal theta in rats there is an emerging phase shift between theta in different layers. The phase difference is about 180° between theta in CA1 and theta in dentate gyrus. Characteristics of this shift differ depending on the rat's state. In freely moving rats there is a notable gradual shift of phase depending on the

depth, whereas in curarized rats it is rather an abrupt reversal of phase occurring in stratum radiatum. Distribution of theta is clearly a species-dependent issue, e.g. in rabbits there is no reported effect of curare on theta profile at all. (O'Keefe and Nadel, 1978)

Another state of EEG was described by Wolansky et al. (2006), who reports so called *hippocampal slow oscillation* recorded using extracellular field techniques in naturally sleeping and urethane-anesthetized rats. This state is present during deactivated stages of sleep and anesthesia and is characteristic by a prominent large-amplitude oscillation with a slow frequency ($\leq 1Hz$). Recorded units exhibited differential firing patterns in different EEG states.

Theta rhytm generation

There are at least two generators of theta rhytm found in the dorsal hippocampus: one is located superficially in CA1, whereas the other one is located ventrally in the stratum lacunosum-moleculare of CA1 and stratum moleculare of the dentate gyrus (Green and Rawlins, 1979). GABAergic and cholinergic neurons of the *medial septum - diagonal band of Broca* contribute to the theta rhythm by feed-forward disinhibition of CA1 pyramidal cells via the interneurons, and cholinergic activation of an intrahippocampal CA3 theta oscillator (Buzsaki, 2002).

Hippocampal feedback to the medial septum is crucial for producing widespread synchrony, however, the hippocampo–septal feedback path is established by long-range GABAergic interneurons. The septal and intrahippocampal pathways produce a current source in the CA1 pyramidal layer and a sink in the stratum radiatum of CA1. Hippocampus also receives rhythmic subcortical modulatory inputs from several other sources (Sirota and Buzsaki, 2005).

Presence of multiple interdependent dipoles was also confirmed in Montgomery et al. (2009) by measured layer-dependent fluctuations of theta power, coherence and phase. Nevertheless, current research points out several inadequacies of this model. One of the findings which is at odds with the described model is that the theta phase relationship of pyramidal cells is not fixed but changes dynamically as a function of behavior (Buzsaki, 2002).

According to its resistance to administration of atropine, two types of theta can be distinguished: atropine-sensitive and atropine-resistant. Early observations reported total elimination of theta oscillations in anesthetized animals. In contrast, in the awake rats the amplitude and frequency of theta rhytm do not substantially change even after large doses of systemically administered muscarinic blockers, although the wave shape and depth profile of theta under at-

ropine are quantitatively different from those in thé drug-free animal. This persisting form of theta is called "atropine resistant" (Buzsaki, 2002).

Another, extrahippocampal, theta oscillator is located in the entorhinal cortex. Perforant path input to distal dendrites of the CA1 and CA3 pyramidal cells and dentate granule cells is expected to produce current dipoles that are responsible for the large amplitude of theta at around the hippocampal fissure (Sirota and Buzsaki, 2005).

Gamma rhytm

Gamma rhytm is usually defined as EEG rhythm at frequencies of 30-100 Hz. Gamma is prominent in the hippocampus during its theta state. Rhythms at similar frequencies occur in the neocortex and they are believed to play an important role in information processing. Gamma rhytm can be artificially generated in vitro by networks of interneurones from CAl stratum oriens and stratum pyramidale during blockade of ionotropic glutamate receptors. Comparable network activity was observed in a model of mutually inhibitory neurones. (Traub et al., 1996)

Sharp waves

Sharp waves are irregular waves that originate in field CA3 and spread throughout the hippocampus when animals are alert but immobile or as a component of the sleep EEG. They are described as monophasic potentials of approximately 50–100 ms duration that occur at irregular intervals when animal enters a state of alert immobility or during the slow-wave portion of sleep. The waves have a mean frequency between 0.5 to 5 Hz and carry a high frequency, low amplitude oscillation (*ripple*) on their ascending phase. (Rex et al., 2009).

It was reported that sharp waves are generated within appropriately prepared hippocampal slices, which confirmed its intrinsic nature. Works on this basis established that sharp waves are composite excitatory potentials generated within CA3 and propagated along that region's associational system. Waves are shaped by strong inhibition, which limits the number of participating cells. These observations strongly suggest that individual sharp waves occur when small populations of neighboring pyramidal cells are recruited by local associational connections into near-synchronous discharge, resulting in a population event that propagates from CA3 and into CA1.

There is observable polarity swap of sharp waves present between the stratum pyramidale and the stratum radiatum of CA1 (Buzsaki, 1986).

Triggering mechanism of sharp waves is not known, but the likely source of activity that could trigger sharp waves is in dentate gyrus. It has been demonstrated that the granule cells generate spontaneous waves and that these precede large sharp waves (Rex et al., 2009). Field sharp waves then represent summation of potentials of CA1 and subicular pyramidal cells and dentate granular cells induced mainly by the Schaffer collaterals (Buzsaki, 1986).

Hippocampal synapses

Hippocampal neurons can be divided into two main groups: Excitatory pyramidal cells and inhibitory interneurons. As in visual or frontal cortex, there are two basic types of synapses to be found: Gray Type 1 and Gray Type 2 synapses. Gray Type 2 synapses are inhibitory and can be found on the soma of pyramidal and granule cells, whereas Gray Type 1 synapses are excitatory and are located on dendritic spines. These glutamatergic synapses are involved in very imporant process of **synaptic plasticity** mainly by **long-term potentiation (LTP)** (Andersen et al., 2007).

Extracellular recordings

There are basically two types of recorded units, that can be found in extracellular recordings of hippocampus. Both fire in a synchrony with the hippocampal theta waves, but in a different way.

The first type of unit has a close relation to theta and is usually reffered to as a **theta cell**. These cells increase their firing rate whenever a theta rhythm appears and usually fire in bursts, with each burst locked to a particular phase of the theta cycle. Majority of theta cells are found in CA1 in the stratum oriens, in CA3 in the stratum lucidum/radiatum and moleculare and in fascia dentata within the hilus. This distribution matches very closely the histological distribution of interneurones.

The second type of unit fires in phase with theta under certain circumstances. The phasing of these units to theta appears to depend on some extrinsic source, while the first type is more directly related to theta itself. These units are located in the stratum pyramidale and are considered to be pyramidal cells. This type is usually called a **complex spike cell**. A complex spike is a burst of several spikes within a brief period (inter-spike interval 1.5-6 ms).

Overall comparison of the theta cells and complex spike cells is shown in Table 1.2.

Table 1.2: Differences between theta cells and complex-spike cells in the hippocampus (O'Keefe and Nadel, 1978)

	property	theta cells	complex-spike cells
1.	(a) Complex spikes (b) Simple action potentials	Never Always	All have some All have some
2.	Duration of extracellular negative spike (distorted)	All 0.15-0.25 ms	All 0.3-0.5 ms in single spikes and spikes of complex spikes
3.	Rate of firing most of the time awake and SWS	Almost all > 8/s	All < 12/s, most < 2/s, many off *
4.	Maximum rate of firing	29-147/s, sustained for many seconds	All < 40/s, most < 20/s sustained for less than 2 s *
5.	Patterns of firing	Comparatively regular	Irregular
6.	During theta rhythm in slow waves in paradoxical sleep or awake (a) Rate (b) Phase relations	 At maximum rate if and only if theta rhythm is present Most have clear phase relation	 No simple relation usually < 1/s * Most have clear phase relation
7.	Relation to LIA spike	Almost all fire with bursts	Sometimes fire
8.	Spike heights	Usually < $200\mu V$ (mean = $164\mu V$)	Larger than theta units (mean = $267\mu V$)
9.	Anatomical location in CA1 in CA3 in dentate gyrus	 Stratum pyramidale Stratum oriens Stratum pyramidale Apical dendritic layers Stratum granulosum Hilus of D.G.	 Stratum pyramidale Stratum pyramidale Stratum granulosum

Place cells

Place cell is a name for hippocampal neurons which are characteristic by location-specific firing. Anatomically, place cells are pyramidal cells. Most

recordings of place cells have been made in the dorsal hippocampus, but they have been also found in the ventral hippocampus. This implies that it is a function of the whole structure.

A given place cell is intensely active when the rat's head gets into a specific place in given environment. This place is usually called a **firing field**. Outside a firing field, the firing rate of such a place cell is virtually zero. As described in O'Keefe and Recce (1993), firing of the place cell may or may not include the complex spike pattern, that is characteristic for pyramidal cells.

In a fixed environment, each place cell has a characteristic and stable firing field. There is a good evidence that single place cells can have two firing fields, but the fraction is low (5–10% reported by Muller (1996)) and depends on the apparatus used. (Muller, 1996)

O'Keefe and Recce (1993) also reported a phase shift between the spike bursts in a firing field and the EEG theta activity. One of suggested explanations for this was that the cell acts as a simple oscillator which is turned on for as long as the inputs exceed the firing threshold. The phase shift then would be caused by a slight difference in the firing frequency and theta rhytm. Nevertheless this mechanism fails in explaining why the field firing always begins at a particular phase of the theta cycle and why the phase shift is restricted to 360° or less. Another explanation presented is a possible presence of two oscillators with same amplitude and opposite phases, which fire at the same frequency outside the firing field and with slightly different frequencies inside the field. Cell firing would then be then induced by interference of these sources.

1.3.3 Effect of Urethane on hippocampal neuronal activity

Urethane (ethyl carbamate) has been widely used as an anesthetic in animal experiments. The advantages of urethane in animal anesthesia are that it can be administered by several parenteral routes, produces a long-lasting steady level of surgical anesthesia, and has minimal effects on autonomic and cardiovascular systems (Hara and Harris, 2002).

According to Hara and Harris (2002), administration of urethane results in potentiation of neuronal nicotinic acetylcholine, γ-aminobutyric acid and glycine receptors, and inhibition of NMDA and α-amino-3-hydroxy-5-methyl-4-isoxazole propionic acid receptors. Urethane lacks a single predominant target for its action.

Effect on theta rhythm

Complete surgical removal of the entorhinal cortex results in a loss of one of the theta sources and such lesions renders the remaining theta oscillation atropine sensitive and its depth profile similar to what observed under urethane anesthesia. This shows that the receptors involved in atropine-resistant type of theta are urethane sensitive. It also shows that the atropine-resistant component of hippocampal theta is conveyed by layer III and layer II entorhinal cortical afferents to the CA1, dentate gyrus and CA3 neurons. These pathways contain glutamate and urethane attenuates glutamate release from presynaptic vesicles. It is expected that activation of NMDA receptors is critical for the atropine-resistant form of theta oscillation. (Buzsaki, 2002)

As described in Kramis et al. (1975), hippocampal theta activity consists of two separate components, one component being urethane-sensitive with frequency range of 7-12 Hz and the second component being urethane-resistant with frequency range of 4-7 Hz.

Effect on Hippocampal unit activity

Mercer et al. (1977) examined effect of urethane on hippocampal activity in rats paralyzed with gallamine triethiodide. They report overall suppression of hippocampal unit activity following urethane administration, which partialy recovers in time. The results show presence of two main distinct groups of cells. The first group had shown a long-lasting depression of activity, while the second group had demonstrated partial or even full recovery in activity in times shorter than 1 hour since administration. These results show possibility of significant bias in electrophysiological recordings with urethane as an anesthetic.

It is generally agreed that at the present time no anesthetic or paralytic agent eliminates confounding influences in electrophysiological recordings in the central nervous system.

1.3.4   Effect of NMDA receptor blockers on hippocampus

Hippocampus contains a class of receptors for the excitatory amino acid glutamate, that are activated by *N-methyl-D-aspartate* (NMDA) and that exhibit a dependency on membrane voltage in becoming active only on depolarization. Blockade of these sites does not detectably affect synaptic transmission, but prevents the induction of the hippocampal long-term potentiation.

As reported by Morris et al. (1986), chronic blockade of NMDA receptor causes a selective impairment of place learning, which is highly sensitive to hip-

pocampal damage (Morris et al., 1982). This shows that the NMDA receptors are involved in spatial learning and supports the hypothesis that LTP is involved in some forms of learning. This was confirmed by Steele and Morris (1999), who found an impairing effect of blocade of intrahippocampal NMDA receptors with D-AP5 on the matching-to-place task.

Kentros et al. (1998) described influence of the NMDA receptors blockade on hippocampal place cells. He reports that there is no effect of the blockade on a formation and a short-term stability of the place cell's firing fields. By contrast the blockade had shown abolition of a long-term stability of the newly established firing fields.

Dizocilpine (MK-801) as the animal model of schizophrenia

Dizocilpine (MK-801) is a non-competitive antagonist of NMDA receptors. It is used to create an animal model of schizophrenia (Nilsson et al., 2001). Unlike dopaminergic agonist, which mimic only the positive symptoms of schizophrenia, MK-801 models both positive (hallucinations, delusions, thought disoder) and negative (amotivation, flattened affect) symptoms (Rung et al., 2005). It was also reported (Eyjolfsson et al., 2006) that repeated administration of a higher dose also induces neurochemical alteration that can be found in first-episode schizophrenic patients.

Bubenikova-Valesova et al. (2008) state that increased cellular destruction by apoptosis or changes in function of glutamatergic NMDA receptors in the early development of central nervous system are decisive for subsequent development of schizophrenia.

Chapter 2

Aim of this thesis

This thesis describes experimental work made on the Department of Neurophysiology of Memory on the Institute of Physiology, Academy of Sciences, Czech Republic in years 2009 and 2010.

Experiments consisted of extracellular recordings of neuronal activity in hippocampus in anaesthetized rats. The basic objective of the experiments was to establish a basic setup for this kind of work and achieve enough practice in this field.

The thesis discusses the effect of administration of dizocilpine (MK-801) on the unit activity in rat's hippocampus. MK-801 has been widely used in behavioral experiments performed in the department and there is a good knowledge base about its effect on behavior. Experiments described in this thesis aimed to uncover details about neural substrate of these changes.

The thesis also discusses the influence of cluster analysis approaches on the reported results as well as the importance of cluster quality.

Chapter 3

Method

3.1 Subjects

The subjects (n=5) were male Long-Evans rats. The rats were obtained from the breeding colony of the Institute of Physiology, Czech Academy of Sciences and housed in a temperature-controlled room (21°C) with a 12:12 light/dark cycle. Rats were kept on standard diet with ad-libitum access to food and water. All procedures were in accordance with Institutional and NIH guidelines and the directive of the European Communities Council (86/609/EEC).

3.1.1 Surgery

One night before the experiment the food was taken away to easy the anaesthetization process. Rats were anaesthetized with a peritoneal administration of 20% solution of Urethane with the dose of 1g/kg. The anaesthetic dose was not administered at once, but it was divided into three or four parts, which were administered in intervals according to the actual progression of the anaesthesis.

After a sufficient anaesthesis was reached, the rat's brain was surgically exposed. Dorsal (parietal) part of the rat's head was shaved and the head was fixed in a stereotaxic apparatus. Skin in the shaved part was cut and periostal layers were removed in order to expose the scull bone.

One hole above each hippocampus was drilled using a bone drill (diameter 3mm) in the coordinates approx. 4mm posterior, 2.5mm lateral from bregma. Holes for the reference electrodes were made with a drill (diameter 1mm) approx. 2-3mm posterior from the hippocampal holes.

After the bone was drilled, dura mater was carefully removed using a sharp pin and forceps. Occasional bleeding was stopped using cotton pads.

As the result of the surgery there were two holes, one above each hippocampus, with clean intact brain exposed and two additional holes for references. Schematic drawing can be seen in Figure 3.1.

3.2 Apparatus

Recording apparatus consisted of the following parts:

1. Follower (made in our laboratory) with tetrode and reference electrode,

2. connecting and switching panel (made in our laboratory),

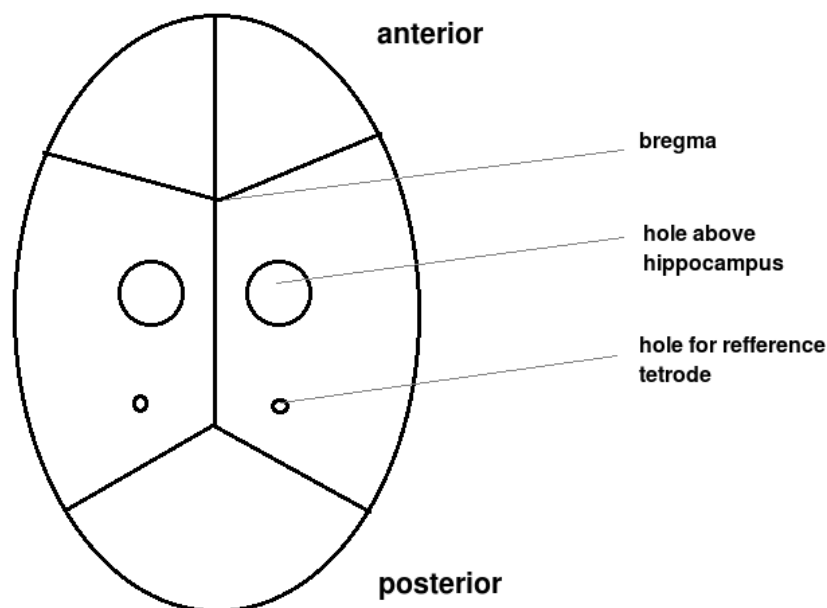3. two eight-channel amplifiers Lynx-8 from Neuralynx Inc.,

Figure 3.1: Schematic drawing of the exposed rat's scull after surgery.

4. A/D converter DataTranslation DT 3110 working with the 32 kHz sampling frequency on 32 channels,

5. oscilloscope with speaker for optical and audio control of the unit activity,

6. recording PC with installed software AcX version 40 or 41 (a software developed for our laboratory).

Tetrode and the reference electrode were attached to the follower and fixed in the stereotaxic aparatus above the rat's head. Follower was connected with the switching panel using a 24-channel thin cable. The switching panel allowed to choose from references and to rearrange the connection between channels before the signal entered the amplifiers.

Follower was connected to the power supply from a set of eight 1.5V batteries and served as a impedance attenuator improving the current source properties.

Amplifiers were controlled using a PC program, the amplification was usually set in the range from 10.000 - 20.000 times. Amplifiers worked also as filters of unwanted high and low frequencies (low cut: 300-600 Hz, high cut: 6000 Hz).

The stereotaxic apparatus with the rat was shielded using metal plates and grounded to a floating groud defined by the follower current source (so called **rat's ground**).

3.3 Electrode assembly

Tetrodes were assembled manually using the Tetrode Assembly Station from Neuralynx Inc. Tetrode channels were made from the Ni-Chrome coated wire, 0.007" bare, 0.001" coating. Assembly cosisted of these steps:

1. Two electrode wires, approx. 15cm each were prepared and the coating at the ends was removed using a hot solder tip.

2. Steel pins were attached to the ends of each wire using a rubber tube (four pins together).

3. Wires were bent in half, hang on the stand by the end with the pins and winded together. The winding was made with 15 coils per centimeter of the original wire plus 10 more coils and 10 coils relaxation.

4. Bundle was fixed together using a heat gun with temperature set to 350°C. Wires were exposed to the hot air twice for approx. 5 seconds each. Hot air caused the coating to melt and glue the wires together.

5. The bent end of the wires was cut using designated tetrode cutting scissors, creating four bare recording tips.

6. Coating quality and integrity was tested by electrolysis in the natrium chloride solution. Each channel was connected as a cathode. As the result, hydrogene bubbles evolved at the tip of the tetrode. In the case of damaged coating, release of hydrogene could be observed elsewhere along the tetrode.

7. Impedance of each channel was measured; if it was too high then another cut of the tip was made. In some cases the impedance was decreased by electrolytic gold plating in a designated gold plating solution. Each channel was exposed in the solution to the voltage of 4.5V for 3-5 seconds. The impedance of a bare electrode was usually about $1M\Omega$, goldened electrodes had the impedance about approx. $300k\Omega$.

8. Final tetrode bundle was fixed in a steel hypotube with the diameter of 31 Ga, using a drop of glue.

9. Steel pins were attached to the mill-max connector and the prepared tetrode was kept for future use safe in a glass bowl fixed with plasticine.

Reference electrode was made from a single coated wire $80\mu m$ in diameter. Steel pin was attached to the end of the wire using a rubber tube.

3.4 Recording

Data were recorded in sessions of the length from 1 to 3 hours according to the current conditions. During the recording the rat was kept on a heating pad (SuperTech Temperature Controller TMP-5a) with the temperature set to 37°C and its body was thermally protected with a blanket from cellulose towels.

To prevent dehydratation a dose of saline (1ml) was aministered intraperitoneally every 1-2 hours.

3.4.1 Unit lookup

Before the recording could start, unit activity had to be found. Tetrode was lowered to the surface of the brain (level 0). Using a microdrive shift the tetrode was lowered quickly 1.5 mm deep to get below neocortex. Then it was moved slowly until a unit activity was observed on the oscilloscope and heard in the speaker.

Unit activity could be observed on the oscilloscope as a typical spike-formed wave and it could be heard in the speaker as sudden cracks emerging in a white noise. Anatomical location of the tetrode tip was estimated from the known coordinates and from the presence of complex spiking neurones arranged in a thin layer (the CA1 part of the hippocampus).

3.4.2 AcX recording software

AcX is a specialized software developed for our laboratory for the purpose of electrophysiological recordings. It allows for variable experimental setups and it is capable to record from multiple tetrodes and to save the EEG continuous signal. It allows the operator to save timestamps of chosen events identified by key presses as well.

AcX performs *discontinuous recording*. It saves a window of 32 samples containing the detected spike. The sampling frequency of the tetrode signal is 32 kHz and therefore the window width is 1ms.

Spikes are detected by comparing the signal value with a preset threshold value. Threshold crossings are detected on all channels and the spike window is started 8 samples back before the detected threshold crossing (data are stored in a cyclic buffer).

Before the recording, threshold values for each channel could be adapted according to the observed noise level to reduce the amount of unwanted data.

Data were stored in a file format containing data structure description in the ascii head and the binary data together (AcX version 40). In AcX version 41 the data were saved in two separate files, one containing the data structure description in XML format and the other containing the binary data.

3.4.3 Drug administration

Solution of MK-801 in saline (0.1mg/ml) was administered intraperitoneally with the dose of 1ml/kg of the animal weight (0.1mg/kg MK-801).

3.5 End of the experiment

After the recording was finished, the apparatus was disassembled and the rat was sacrificed and its brain was removed and stored in a formaldehyde solution for future histological verification of electrode position.

3.6 Data processing

Recorded data were processed using manual, semi-automatic and automatic cluster analysis. The manual clustering was made in the MClust version 3.5 and Matlab version 2008b. The automatic clustering was made with the KlustaKwik version 1.5 program, the semi-automatic clustering was a combination of KlustaKwik and MClust. In the semi-automatic clustering the only operations that were allowed were either to remove the cluster or to join several clusters together.

To allow a processing of the data in MClust it was necessary to develop a loading engine function. This function had to transform the recorded data from the AcX software format to the format demanded by MClust. This was done by the author of this thesis with special attention to the speed performance in cases of large data files.

As the MClust allows for the feature calculation, it was used for this purpose. Features were chosen according to the current need, usualy including *peak* and *energy* for each channel.

The KlustaKwik program was used configured with the following parameters

```
-MinClusters 2 -MaxClusters 10 -MaxPossibleClusters 10
```

The produced clustering was further analysed and evaluated using a set of Matlab functions written by the author of this thesis.

Cluster quality

The quality of the clusters was evaluated using the L-ratio and Isolation distance metrics. Implementations of these functions are distributed together with the MClust software and they were used by us without changes. Schmitzer-Torbert et al. (2005) suggest to use a threshold to define the minimum value of each cluster quality measure in order for a unit to be considered in further analyses. There is no recommended threshold value, in this thesis I decided to consider clusters with L-ratio < 0.1 and Isolation distance > 20 as good.

Cell type

The cell type represented by a cluster was estimated according to the properties described in the Table 1.2. A cluster was assigned to one of three possible cell types:

- **Complex-spike cell** for clusters with the average firing rate < 2 Hz and the average spike width > 300 μs.

- **Theta cell** for clusters with the average firing rate > 8 Hz and the average spike width < 250 μs.

- **Undecided** for the clusters that did not fall into any of the previous categories.

Firing rate

Firing rate was calculated as a frequency of spikes in a chosen time frame (60 or 300 seconds), producing a series of values for the underlying data. The differences of firing rates before and after the drug administration were statistically tested using the Mann-Whitney U-test.

Kendall τ

Kendall τ correlation coefficient (Press et al., 2007) was calculated using the Matlab corr function in a chosen time frame (300 s). Each time frame was divided into separate time bins of 250 ms, in which the number of spikes was compared by the algorithm.

Chapter 4

Results

4.1 Recording of hippocampal neuronal activity in anaesthetized rats

In this section I present recordings of the hippocampal neuronal activity. The effect of different clustering approaches on the overall cluster quality is compared here.

The neuronal activity was recorded in one rat (Subject 1) at two different locations. Data were clustered using manual, semi-automatic and automatic clustering.

4.1.1 Recording 1

The first recording started 4 hours and 12 minutes after finishing the surgery and its duration was 36 minutes. The tetrode tip was located in the left hippocampus on the coordinates 2.5 mm mediolateral, 3.5 mm posterior from bregma and 2.45 mm ventral. From the coordinates and the observed activity it was estimated that the tip was in the CA1 part of the hippocampus.

The manual as well as the semi-automatic clustering of the recorded data produced three clusters, whereas the automatic clustering in the KlustaKwik program produced ten clusters. KlustaKwik reached the maximum number of clusters allowed by its configuration and clustered all the spikes present, including the spikes that were considered as a noise in the manual clustering.

The cluster quality was compared using L-ratio and Isolation distance measures. List of all the clusters and their quality measures is presented in the Table 4.1.

To compare the overall quality of the clusterings, mean and standard deviation of the L-ratio and the Isolation distance were calculated for each clustering. The values are listed in Table 4.2. Comparing the cluster quality measures with the chosen threshold (L-ratio < 0.1 and Isolation distance > 20) there is one good cluster in manual clustering, two good clusters in semi-automatic clustering and five good clusters in automatic clustering.

To illustrate the differences in the clusterings I also present a scatter-plot of the unclustered data (Figure 4.1) and the same scatter-plot after each of the clusterings (Figures 4.2, 4.3 and 4.4).

Cluster	L-ratio	Isolation distance	Good
M1	0.003	-	*
M2	0.149	26.340	
M3	0.174	26.362	
S1	0.022	24.968	*
S2	0.001	-	*
S3	0.702	11.253	
A1	-	-	
A2	0.022	24.968	*
A3	0.458	13.484	
A4	0.043	26.570	*
A5	29.392	4.113	
A6	0.010	48.179	*
A7	0.001	-	*
A8	0.702	11.253	
A9	0.097	20.643	*
A10	7.934	2.990	

Table 4.1: Cluster quality comparison for the recording 1. Clusters marked M are from the manual clustering, clusters marked S are from the semi-automatic clustering and clusters marked A are from the automatic clustering. Dash instead of a value marks an undefined value. The last column indicates which clusters met the conditions for a good cluster (L-ratio < 0.1 and Isolation distance > 20).

Clustering	L-ratio	Isolation distance
Manual	0.109 ± 0.092	26.351 ± 0.016
Semi-automatic	0.241 ± 0.399	18.111 ± 9.698
Automatic	4.295 ± 9.757	19.025 ± 14.714

Table 4.2: Clustering quality properties for the recording 1. Each row contains means and standard deviations of the respective measures calculated from all the clusters produced by the clustering.
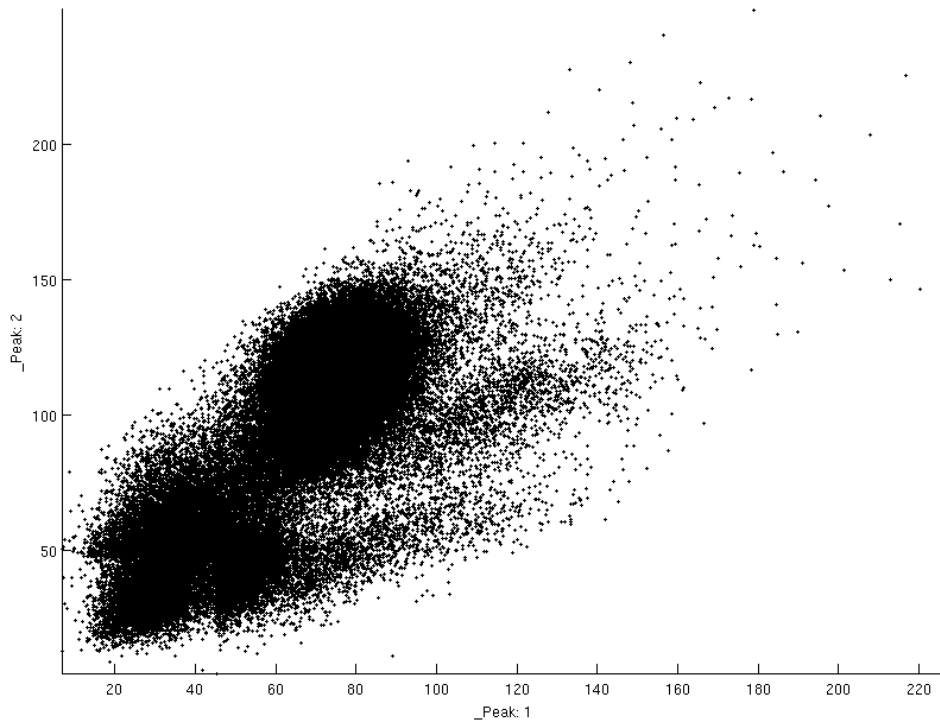
Figure 4.1: Scatter-plot example of the unclustered data, recording 1. Features Peak1 and Peak2 reffer to the peak on channels 1 and 2.
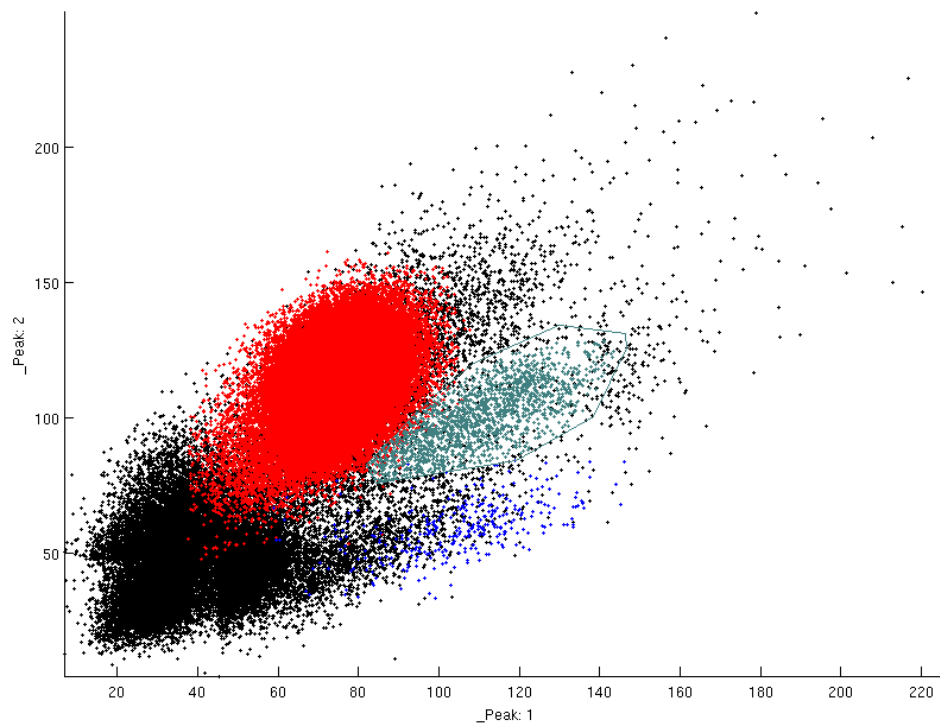

Figure 4.2: Scatter-plot example of the manual clustering, recording 1. Features Peak1 and Peak2 reffer to the peak on channels 1 and 2.
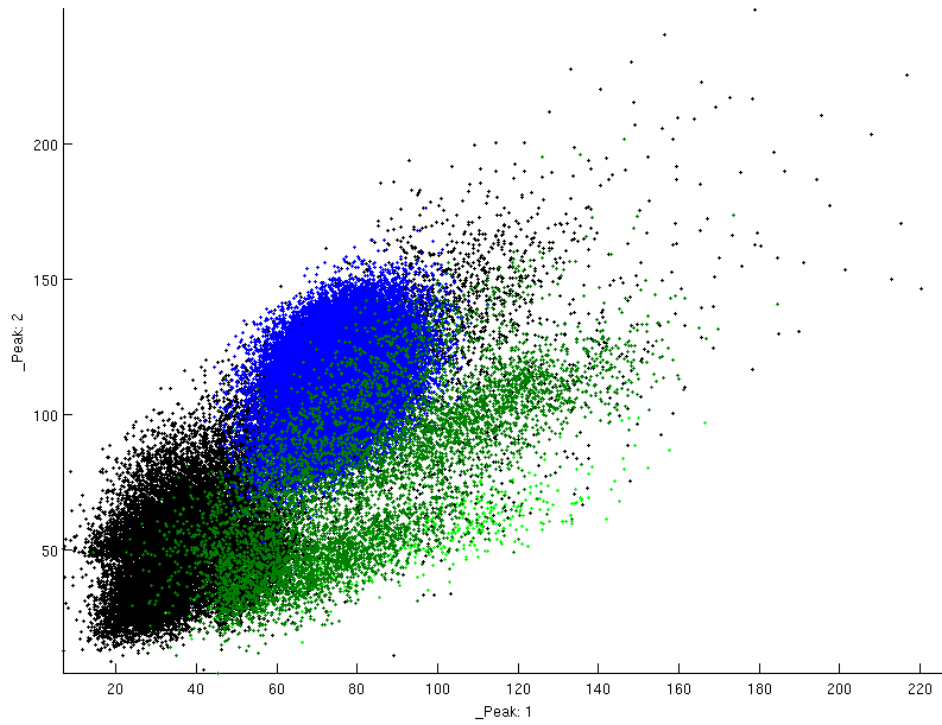
Figure 4.3: Scatter-plot example of the semi-automatic clustering, recording 1. Features Peak1 and Peak2 reffer to the peak on channels 1 and 2.
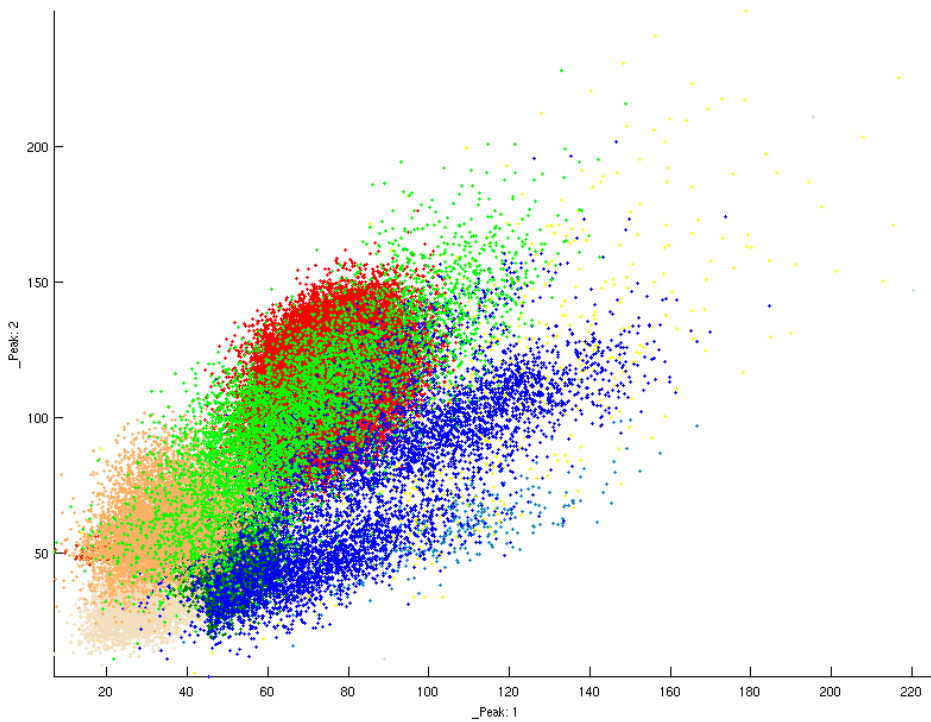

Figure 4.4: Scatter-plot example of the automatic clustering, recording 1. Features Peak1 and Peak2 reffer to the peak on channels 1 and 2.

4.1.2 Recording 2

The second recording started 5 hours and 2 minutes after finishing the surgery and its duration was 32 minutes. The tetrode tip was located in the left hippocampus on the coordinates 2.5 mm mediolateral, 3.5 mm posterior from bregma and 2.50 mm ventral. From the coordinates and the observed activity it was estimated that the tip was in the CA1 part of the hippocampus.

The manual clustering produced five clusters, the semi-automatic clustering produced four clusters and the automatic clustering in KlustaKwik program produced ten clusters. As in the first recording, KlustaKwik reached the maximum number of clusters allowed by its configuration and clustered all the spikes present, including the spikes that were considered as a noise in the manual clustering.

The cluster quality was compared using L-ratio and Isolation distance measures. List of all the clusters and their quality measures is presented in the Table 4.3.

To compare the overall quality of the clusterings, mean and standard deviation of the L-ratio and the Isolation distance were calculated for each clustering. The values are listed in Table 4.4. Comparing the cluster quality measures with the chosen threshold (L-ratio < 0.1 and Isolation distance) there is no good cluster in the manual clustering and four good clusters in the semi-automatic clustering as well as in the automatic clustering.

To illustrate the differences in the clusterings I also present a scatter-plot of the unclustered data (Figure 4.5) and the same scatter-plot after each of the clusterings (Figures 4.6, 4.7 and 4.8).

Cluster	L-ratio	Isolation distance	Good
M1	0.488	26.124	
M2	0.711	10.727	
M3	1.252	8.071	
M4	0.831	10.139	
M5	0.521	13.733	
S1	0.000	152.971	*
S2	0.019	26.303	*
S3	0.005	49.632	*
S4	0.013	41.584	*
A1	162.828	2.755	
A2	0.188	17.130	
A3	0.000	152.971	*
A4	1.434	10.200	
A5	0.019	26.303	*
A6	0.744	12.038	
A7	0.005	49.632	*
A8	7.137	3.314	
A9	0.013	41.584	*
A10	11.725	3.495	

Table 4.3: Cluster quality comparison for the recording 2. Clusters marked M are from the manual clustering, clusters marked S are from the semi-automatic clustering and clusters marked A are from the automatic clustering. The last column indicates which clusters met the conditions for a good cluster (L-ratio < 0.1 and Isolation distance > 20).

Clustering	L-ratio	Isolation distance
Manual	0.760 ± 0.308	13.759 ± 7.203
Semi-automatic	0.009 ± 0.008	67.622 ± 57.716
Automatic	18.409 ± 50.897	31.942 ± 45.527

Table 4.4: Clustering quality properties for the recording 2. Each row contains means and standard deviations of the respective measures calculated from all the clusters produced by the clustering.
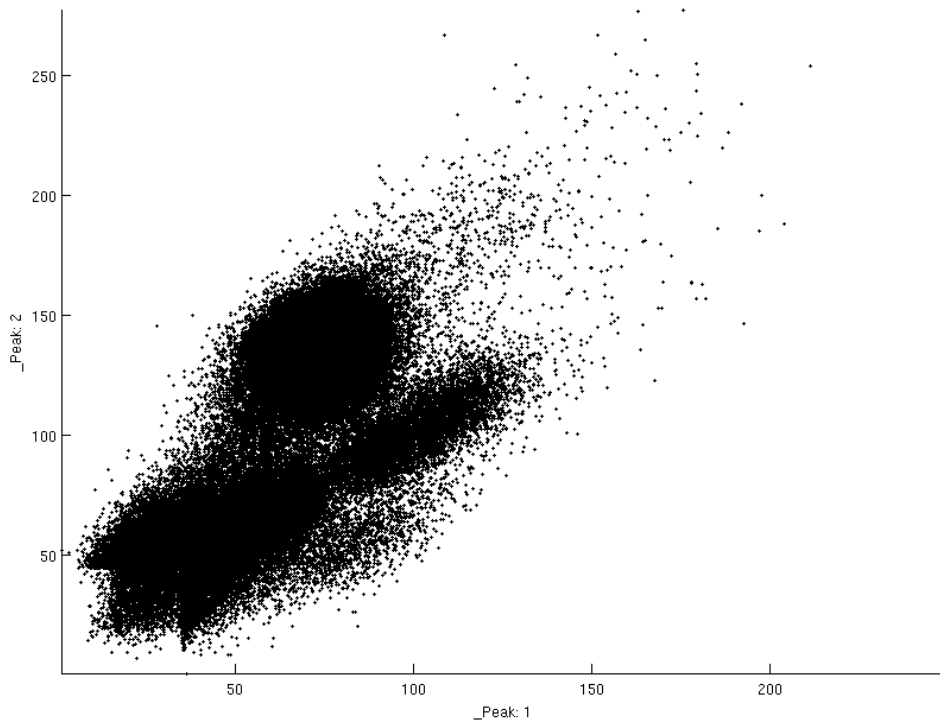
Figure 4.5: Scatter-plot example of the unclustered data, recording 2. Features Peak1 and Peak2 reffer to the peak on channels 1 and 2.
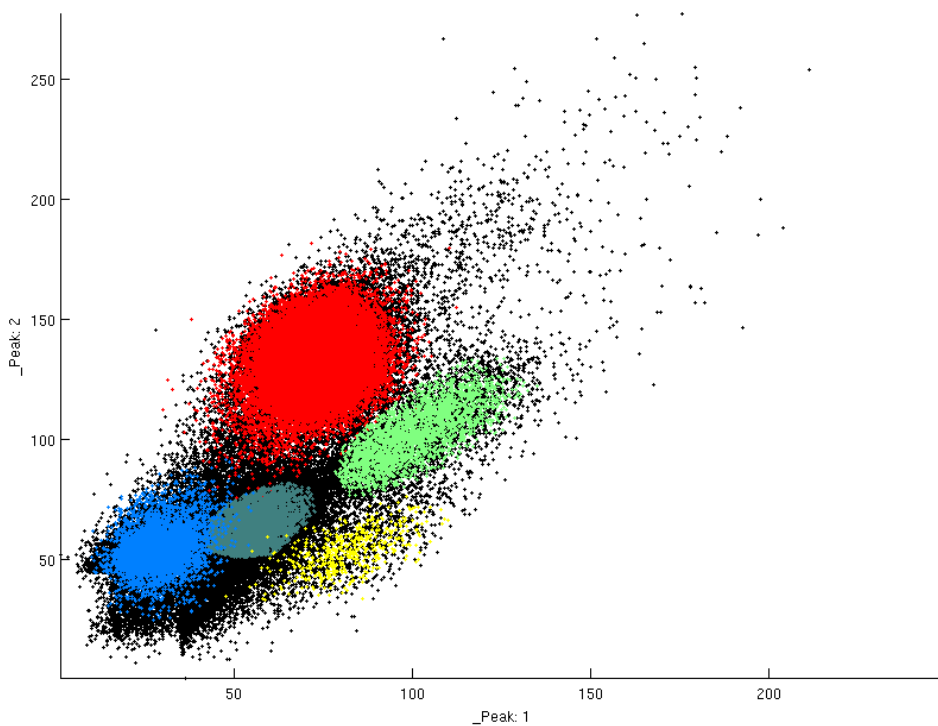

Figure 4.6: Scatter-plot example of the manual clustering, recording 2. Features Peak1 and Peak2 reffer to the peak on channels 1 and 2.
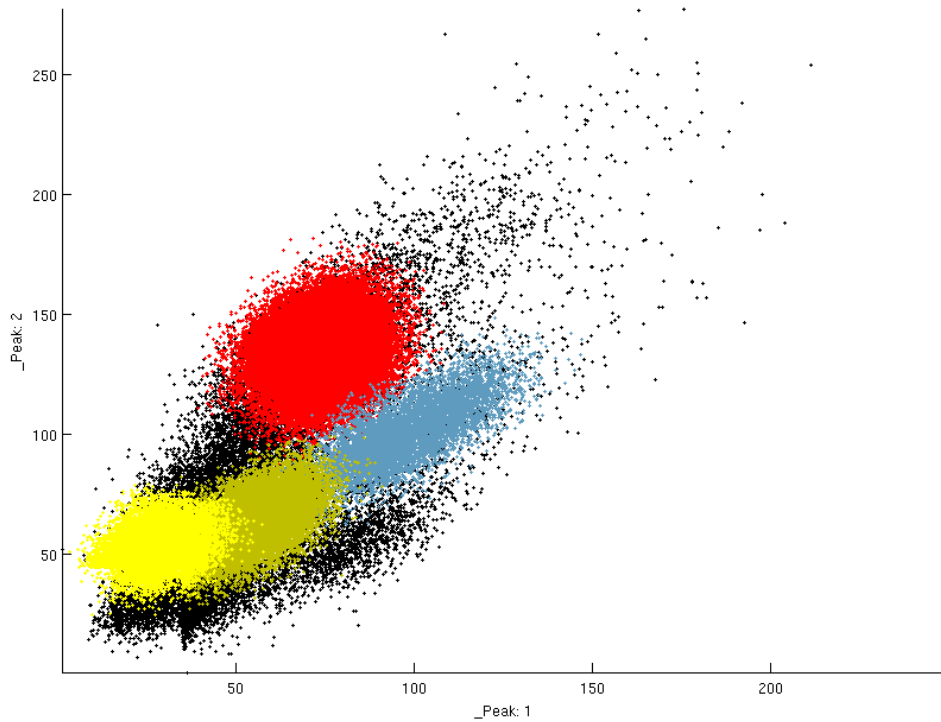
Figure 4.7: Scatter-plot example of the semi-automatic clustering, recording 2. Features Peak1 and Peak2 reffer to the peak on channels 1 and 2.
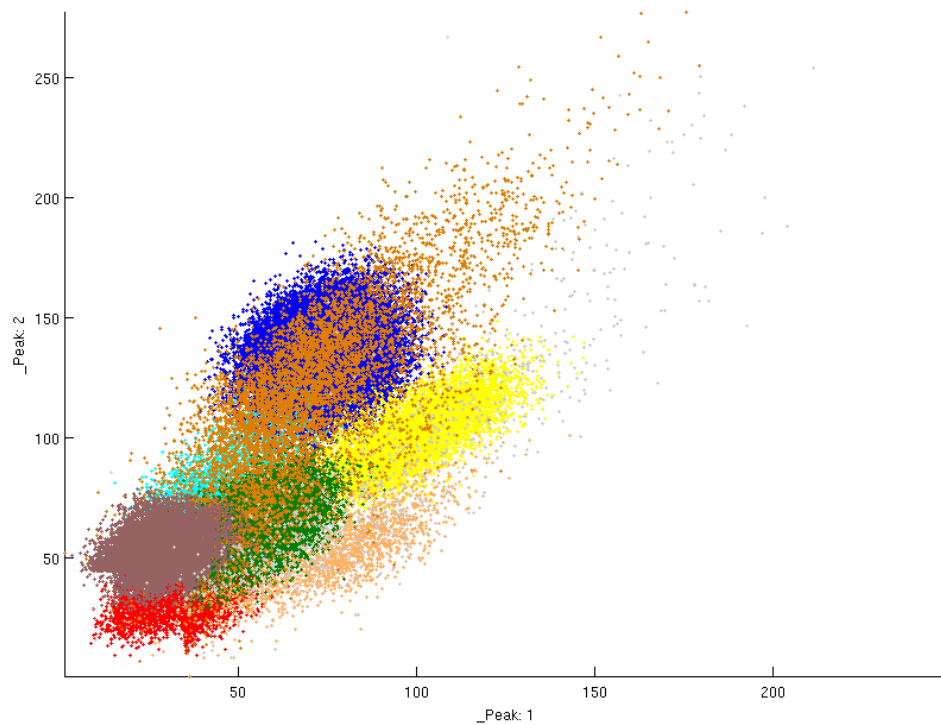

Figure 4.8: Scatter-plot example of the automatic clustering, recording 1. Features Peak1 and Peak2 reffer to the peak on channels 1 and 2.

4.2 Effect of MK-801 on the hippocampal neuronal activity in anaesthetized rats

The effect of the MK-801 on the hippocampal neuronal activity was tested in four rats (Subject 2-5). However two subjects were excluded from further analysis. One rat (Subject 4) was excluded, because the recorded activity was unclusterable. The other rat (Subject 5) was excluded from the evaluation because the recording was unstable.

4.2.1 Overall activity

The firing frequency of all the events which crossed the threshold before and after administration of MK-801 was compared by Mann-Whitney U-test. The frequency was calculated in 300 s successive time frames. In both recordings there was an observed rise of activity after administration of MK-801. The progression of the firing frequency for Subject 2 is shown in Figure 4.9 and for Subject 3 in Figure 4.10. Overview of the average firing rates is listed in Table 4.5.
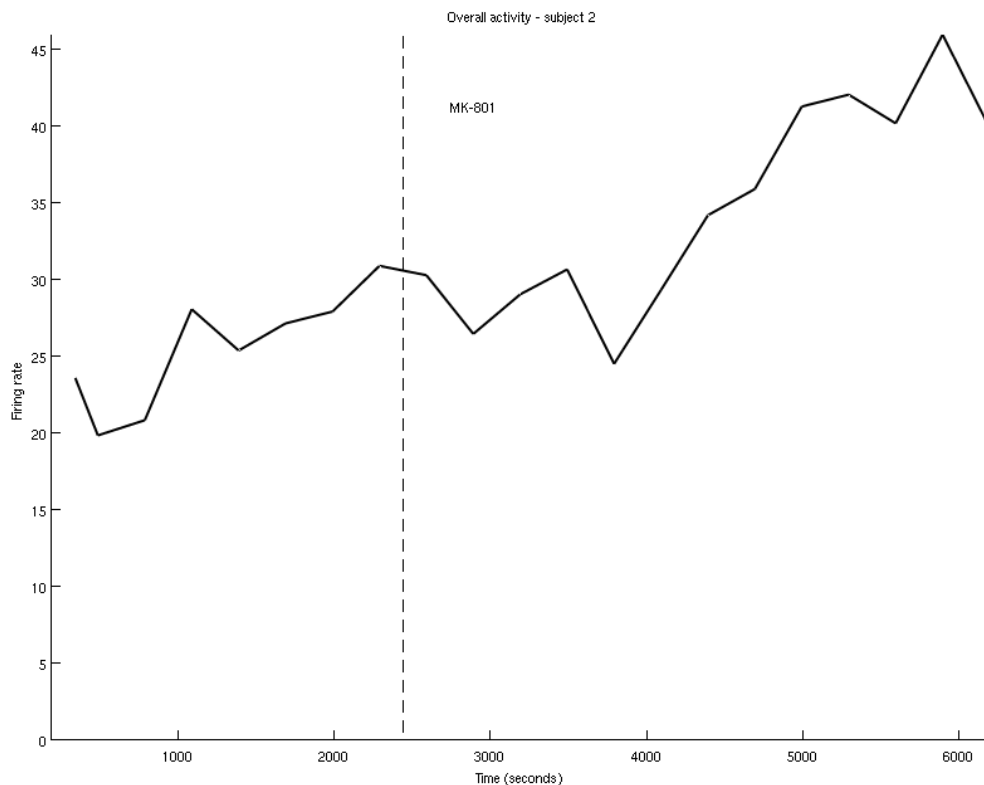

Figure 4.9: Overall unit activity, subject 2. Dashed line marks administration of MK-801.
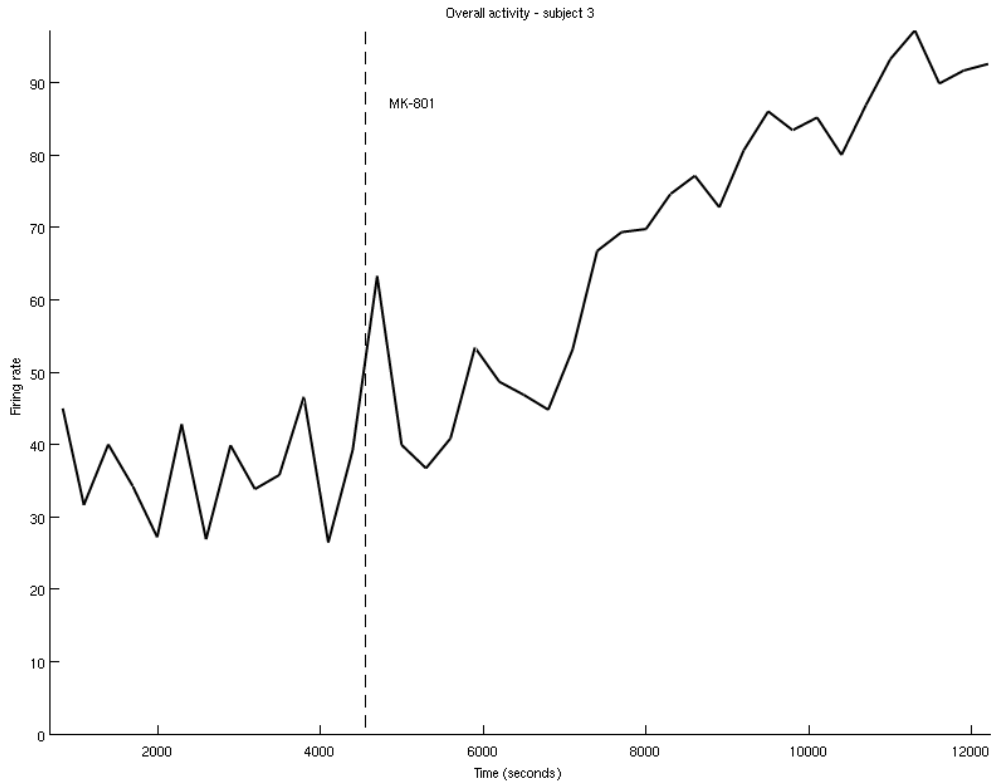
Figure 4.10: Overall unit activity, subject 3. Dashed line marks administration of MK-801.

Subject	FR-pre	FR-post	p-value	
2	25.458 ± 3.805	34.586 ± 6.771	0.0053	**
3	36.239 ± 6.811	70.257 ± 18.954	**4.81E-06**	**

Table 4.5: Overview of the overall unit activity comparison. FR-pre is mean and standard deviation of the firing rate before administration of MK-801, FR-post is mean and standard deviation of the firing rate after administration; p-value is the Mann-Whitney U-test statistics; ** mark results significantly different on the h=0.01 significance level.

4.2.2 Recorded units

Recordings from subjects 2 and 3 were clustered in three ways: Manual clustering by two independent operators (here reffered to as operator A and operator B) and by a semi-automatic clustering based on the KlustaKwik results. Clusters from manual clustering of operator A are marked MA, clusters from manual clustering of operator B are marked MB, clusters from semi-automatic clustering are marked SK.

Cluster quality was evaluated using L-ratio and Isolation distance quality measures. Only clusters with the L-ratio < 0.1 and the Isolation distance > 20 were used for evaluation.

The cell type was estimated according to the properties described in Table 1.2. Clusters with the average firing rate < 2 Hz and the average spike width > 300 μs were considered as complex-spike cells, clusters with the average firing rate > 8 Hz and the average spike width < 250 μs were considered as theta cells. Clusters that did not fall into any of the previous groups were considered as an undecided cell type.

The presence of inter-spike intervals shorter than the absolute refractory period (1 ms) was calculated and is presented as an additional parameter of the cluster quality.

The operator A created 6 clusters for subject 2 and 5 clusters for subject 3; the operator B created 8 clusters for subject 2 and 5 clusters for subject 3; semi-automatic clustering produced 4 clusters for subject 2 and 5 clusters for subject 3. Results from the presented clusterings including cluster quality assessment are shown in Tables 4.6, 4.7 and 4.8.

Subject	Cluster	L-ratio	Isol. dist	%ISI < 1ms	Cell type	Evaluated
2	MA21	0.047	37.407	0	CSC	*
2	MA22	0.037	48.365	0	-	*
2	MA23	0.078	26.259	0	-	*
2	MA24	0.049	39.864	0	CSC	*
2	MA25	0.231	17.178	0	CSC	
2	MA26	0.038	48.444	0	-	*
3	MA31	0.438	15.758	0.827	CSC	
3	MA32	0.044	25.054	1.102	-	*
3	MA33	0.060	39.207	0.709	CSC	*
3	MA34	0.267	17.429	0.433	CSC	
3	MA35	0.328	15.453	1.444	CSC	

Table 4.6: Cluster quality measures, manual clustering, operator A. ISI stands for the inter-spike interval. The estimated cell type can be either CSC (complex-spike cell), TC (theta cell) or dash (undecided). Last column indicates which clusters were used for the further evaluation.

Subject	Cluster	L-ratio	Isol. dist	%ISI < 1ms	Cell type	Evaluated
2	MB21	0.033	44.139	0	-	*
2	MB22	0.091	21.598	0	-	*
2	MB23	0.219	18.242	0	CSC	
2	MB24	0.063	29.020	0	CSC	*
2	MB25	0.127	23.192	0	CSC	
2	MB26	0.498	13.730	0	CSC	
2	MB27	0.651	12.578	0.081	CSC	
2	MB28	0.069	29.943	0	CSC	*
3	MB31	0.054	34.710	0.561	-	*
3	MB32	0.196	18.901	0.642	CSC	
3	MB33	0.060	29.909	0.788	CSC	*
3	MB34	0.302	15.859	1.190	CSC	
3	MB35	0.800	13.856	0.590	CSC	

Table 4.7: Cluster quality measures, manual clustering, operator B. ISI stands for the inter-spike interval. The estimated cell type can be either CSC (complex-spike cell), TC (theta cell) or dash (undecided). Last column indicates which clusters were used for the further evaluation.

Subject	Cluster	L-ratio	Isol. dist	%ISI < 1ms	Cell type	Evaluated
2	SK21	0.364	15.356	0.028	CSC	
2	SK22	0.032	28.449	0	-	*
2	SK23	1.282	9.764	0.167	CSC	
2	SK24	0.091	20.545	0	CSC	*
3	SK31	3.369	9.714	0.988	CSC	
3	SK32	0.082	21.530	0.625	-	*
3	SK33	1.016	10.522	2.159	-	
3	SK34	0.014	28.661	0.716	-	*
3	SK35	9.392	5.887	0.962	CSC	

Table 4.8: Cluster quality measures, semi-automatic clustering based on the KlustaKwik algorithm results. ISI stands for the inter-spike interval. The estimated cell type can be either CSC (complex-spike cell), TC (theta cell) or dash (undecided). Last column indicates which clusters were used for the further evaluation.

Matching clusters

To determine which clusters in different clusterings of the same recording represent the same unit it was neccessary to find the mutually corresponding clusters. Clusters were matched together across the clusterings according to the distances of their centers. Only clusters with the distance of centers below 40 were considered as matching.

The results show that the following clusters are matching (listing only clus-

ters with a good quality that were used for the further evaluation): MA21 + MB24 + SK24, MA22 + MB21, MA23 + MB22, MA24 + MB28, MA32 + MB31 + SK34 and MA33 + MB33.

Distances of all the clusters for subject 2 are shown in Table 4.9, 4.10 and 4.11, distances of all the clusters for subject 3 are shown in Table 4.12, 4.13 and 4.14.

Clusters	MB21	MB22	MB23	MB24	MB25	MB26	MB27	MB28
MA21	482.6	318.1	421.2	**16.6**	221.0	170.8	201.2	654.6
MA22	**11.8**	230.2	433.8	482.6	490.0	477.5	523.9	474.0
MA23	211.7	**11.7**	296.9	319.2	323.8	281.8	327.0	504.6
MA24	489.7	531.0	408.2	664.1	540.1	605.3	657.6	**26.9**
MA25	428.4	292.0	**24.6**	418.4	269.2	300.4	297.7	408.6
MA26	234.0	281.5	538.4	459.8	511.6	478.2	550.7	499.2

Table 4.9: Distances of cluster centers for manual clusterings from operator A and operator B for subject 2. The matching clusters are printed bold.

Clusters	SK21	SK22	SK23	SK24
MA21	396.2	367.2	364.5	20.3
MA22	514.0	158.4	582.0	492.7
MA23	347.2	65.0	388.4	319.2
MA24	540.0	508.0	712.6	673.8
MA25	120.7	331.2	297.0	402.2
MA26	596.4	230.9	636.0	475.2

Table 4.10: Distances of cluster centers for manual clusterings from operator A and semi-automatic clusterings for subject 2. No matching clusters were found.

Clusters	SK21	SK22	SK23	SK24
MB21	503.7	147.2	570.8	483.4
MB22	340.0	71.9	378.7	313.1
MB23	140.9	330.2	319.7	407.7
MB24	402.9	360.9	374.4	**33.9**
MB25	253.1	369.0	300.5	219.5
MB26	265.9	336.2	250.2	153.1
MB27	236.5	380.7	182.1	181.9
MB28	518.0	488.5	691.2	655.1

Table 4.11: Distances of cluster centers for manual clusterings from operator A and semi-automatic clusterings for subject 2. The matching clusters are printed bold.

Clusters	MB31	MB32	MB33	MB34	MB35
MA31	99.3	**3.6**	67.8	79.6	55.8
MA32	**17.8**	85.5	102.8	104.4	88.2
MA33	116.3	70.5	**5.9**	63.0	87.3
MA34	107.1	57.8	83.1	92.7	**7.2**
MA35	121.1	78.6	62.1	**7.7**	88.7

Table 4.12: Distances of cluster centers for manual clusterings from operator A and operator B for subject 3. The matching clusters are printed bold.

Distances	SK31	SK32	SK32	SK34	SK35
MA31	**7.3**	82.7	64.1	99.6	45.6
MA32	78.2	48.7	78.3	**17.8**	78.0
MA33	73.1	118.3	76.7	116.9	52.0
MA34	54.0	81.3	69.9	107.2	51.6
MA35	75.9	103.9	**34.1**	121.4	43.0

Table 4.13: Distances of cluster centers for manual clusterings from operator A and semi-automatic clusterings for subject 3. The matching clusters are printed bold.

Distances	SK31	SK32	SK33	SK34	SK35
MB31	94.2	61.2	95.7	**1.5**	93.9
MB32	**10.3**	85.1	65.9	100.4	46.5
MB33	68.6	113.5	72.0	113.6	47.1
MB34	77.8	106.1	**37.8**	120.2	44.8
MB35	52.3	76.6	66.8	104.1	50.3

Table 4.14: Distances of cluster centers for manual clusterings from operator B and semi-automatic clusterings for subject 3. The matching clusters are printed bold.

4.2.3   Activity of the recorded units

Firing rate

The effect of administration of MK-801 on the unit activity was tested using the firing rate. Firing rate was calculated in 300 s successive time frames and the values before and after administration of MK-801 were compared using the Mann-Whitney U-test.

In all clusterings there was one unit that showed a significant decrease of the firing rate and two units that showed a significant rise of the firing rate on the 0.05 significance level. In all cases the significance and the directon of the change were the same for the matching clusters. The other units showed no

significant change on the 0.05 significance level. Overview of the firing rates and test results is presented in Table 4.15. Firing rate progression for the clusters with a significant change is plotted in Figures 4.11, 4.12, 4.13 and 4.14.

Cluster	FR-pre	FR-post	p-value		
MA21	0.94 ± 0.46	0.13 ± 0.10	1.917E-04	*	↓
MA22	0.22 ± 0.05	0.16 ± 0.07	0.1282		
MA23	0.29 ± 0.40	0.39 ± 0.48	0.2047		
MA24	0.02 ± 0.01	0.03 ± 0.03	0.2912		
MA26	0.01 ± 0.01	0.01 ± 0.04	0.0364		
MA32	6.38 ± 1.13	13.07 ± 3.84	5.538E-06	*	↑
MA33	0.16 ± 0.14	0.38 ± 0.26	0.0037	*	↑
MB21	0.23 ± 0.06	0.18 ± 0.08	0.1681		
MB22	0.37 ± 0.48	0.52 ± 0.58	0.1375		
MB24	1.08 ± 0.45	0.15 ± 0.12	1.908E-04	*	↓
MB31	4.17 ± 0.73	7.26 ± 2.55	4.770E-05	*	↑
MB33	0.16 ± 0.13	0.37 ± 0.25	0.0051	*	↑
SK22	0.66 ± 0.53	0.72 ± 0.61	0.9711		
SK24	1.24 ± 0.50	0.31 ± 0.09	1.881E-04	*	↓
SK32	2.18 ± 2.01	3.53 ± 2.03	1.455E-04	*	↑
SK34	5.20 ± 0.80	9.61 ± 2.61	5.930E-06	*	↑

Table 4.15: Firing rate of the selected clusters. FR-pre is mean + standard deviation of the firing rate before administration of MK-801, FR-post is mean + standard deviation of the firing rate after administration; p-value is Mann-Whitney U-test statistics; fifth column marks statistically significant differences on the 0.05 significance level. The test probability was corrected with the *Bonferroni correction* for multiple comparisons. Last column indicates the direction of change.
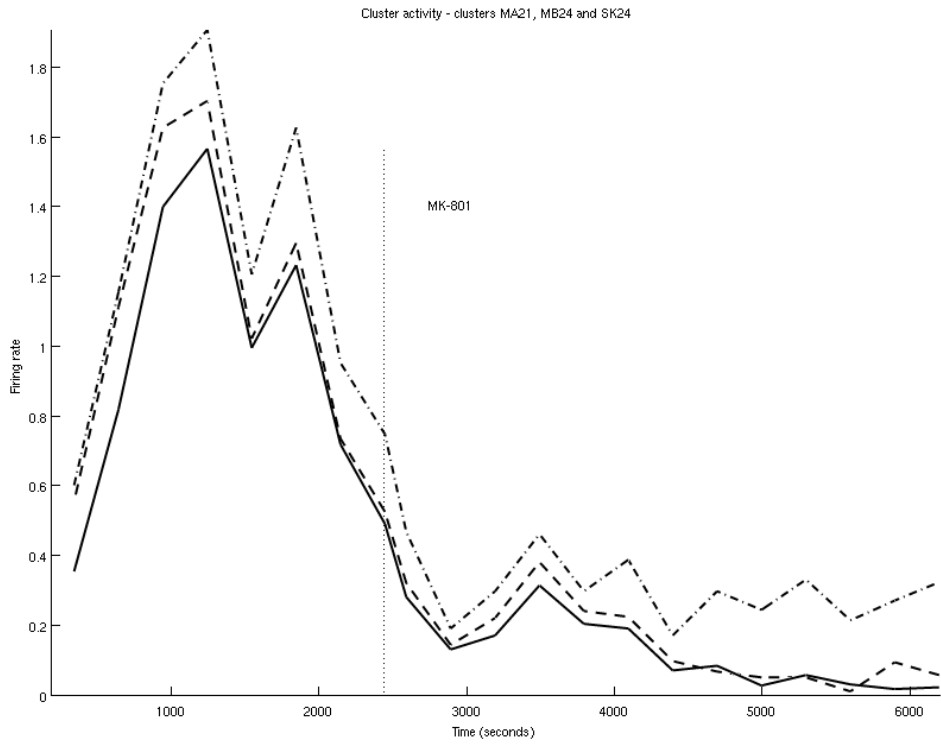
Figure 4.11: Firing rate progression for matching clusters MA21(solid line), MB24 (dashed line) and SK24 (dashed-dotted line).
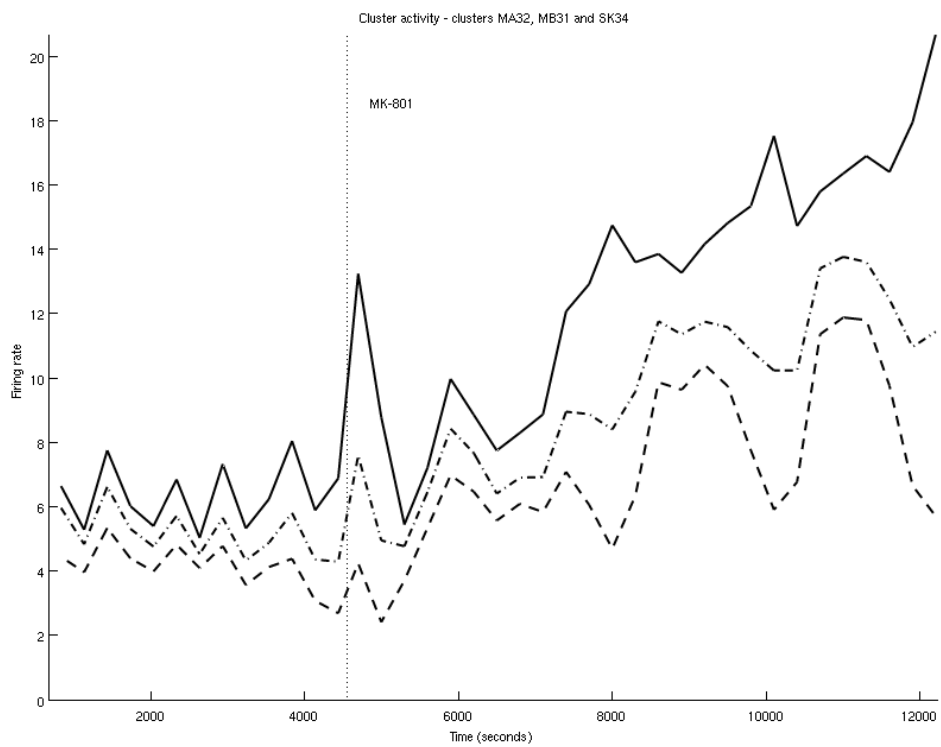

Figure 4.12: Firing rate progression for matching clusters MA32 (solid line), MB31 (dashed line) and SK34 (dashed-dotted line).
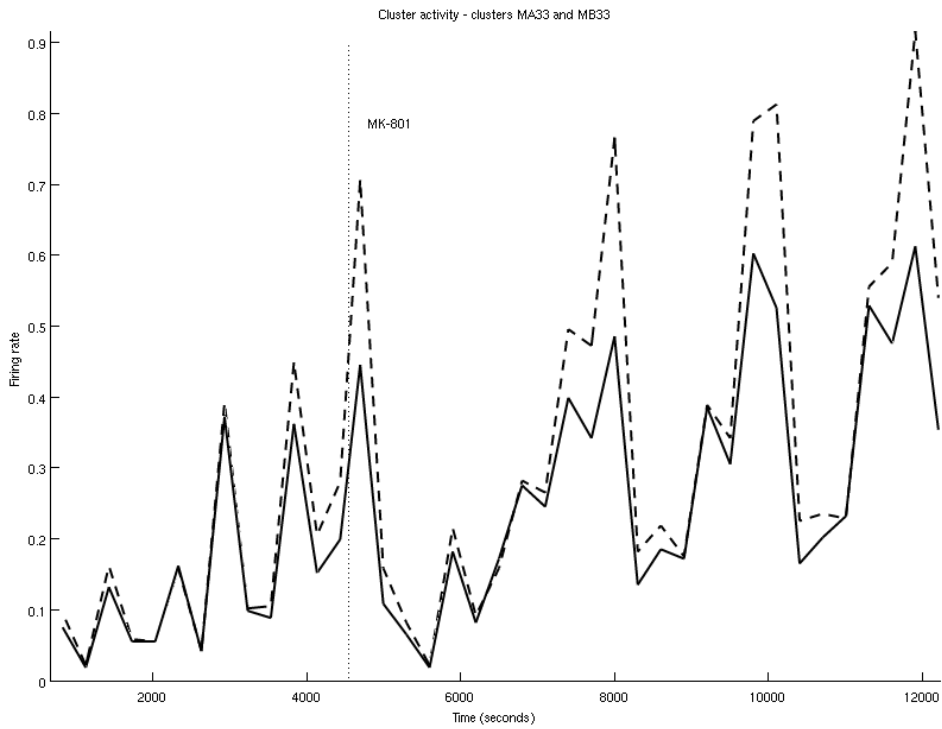
69

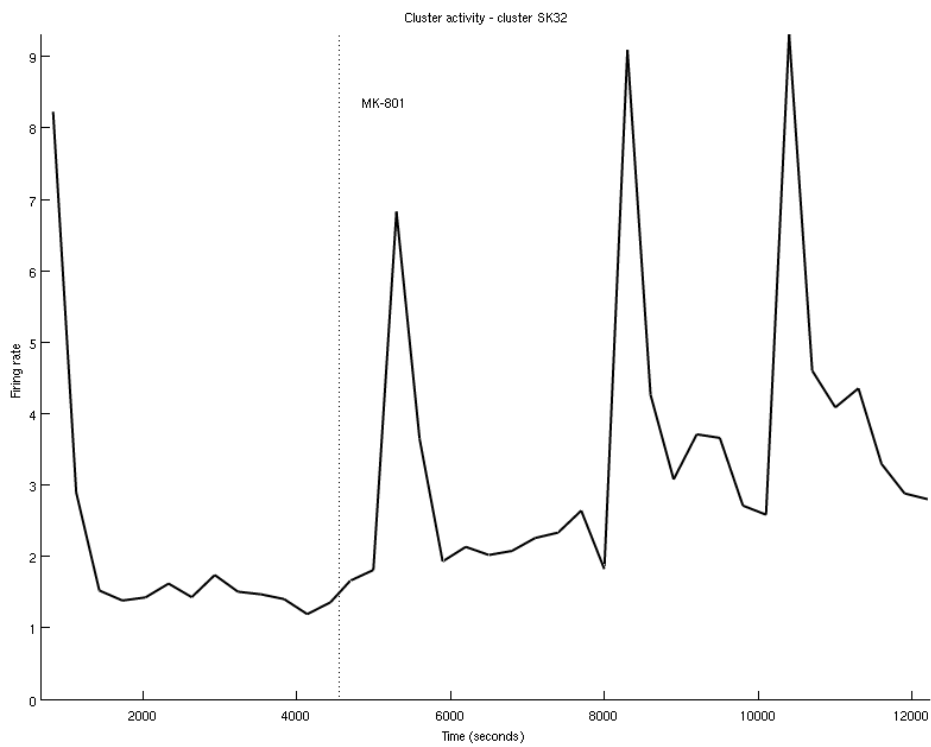Figure 4.13: Firing rate progression for matched clusters MA33 (solid line) and MB33 (dashed line).

Figure 4.14: Firing rate progression for cluster SK32.

Correlation

To evaluate the effect of administration of MK-801 on the mutual correlation of activity of different units, the *Kendall τ* correlation coefficient was used. The coefficient was calculated for 300 s successive time frames. Each frame was divided into bins of 250 ms and the spikes count in the corresponding bins was used for the coefficient calculation.

The correlation was calculated for all the cluster pairs in manual clustering of both operators. The semi-automatic clustering was not used because of the low number of comparable clusters. The means and standard deviations of the coefficients along with the linear regression equation are shown in the presented plots (Figure 4.15, 4.16, 4.17, 4.18, 4.19, 4.20, 4.21 and 4.22). The values are presented partly for all the clusters, partly only for the clusters that met the quality conditions.

The plots show that there is no observed change of correlation in subject 2 and that there is a decrease of correlation in subject 3 that happened with no relation to the administration of MK-801. It can be also seen that the progression of correlation does not remarkably change depending on the cluster quality.
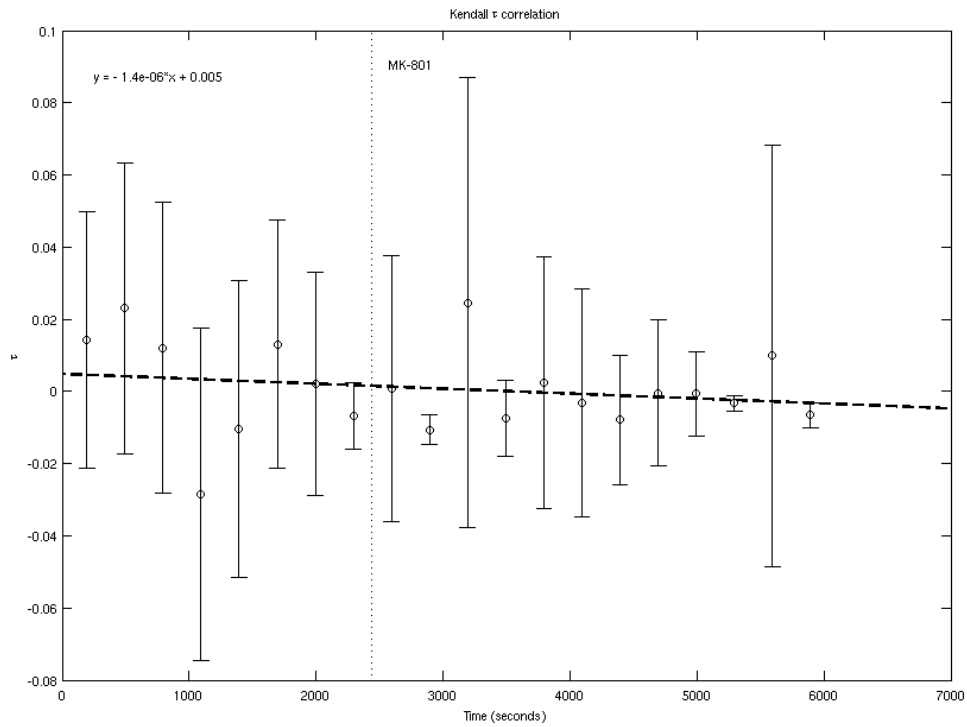
Figure 4.15: Kendall τ correlation of the good clusters (means of all possible couples) from the manual clustering of operator A for subject 2.
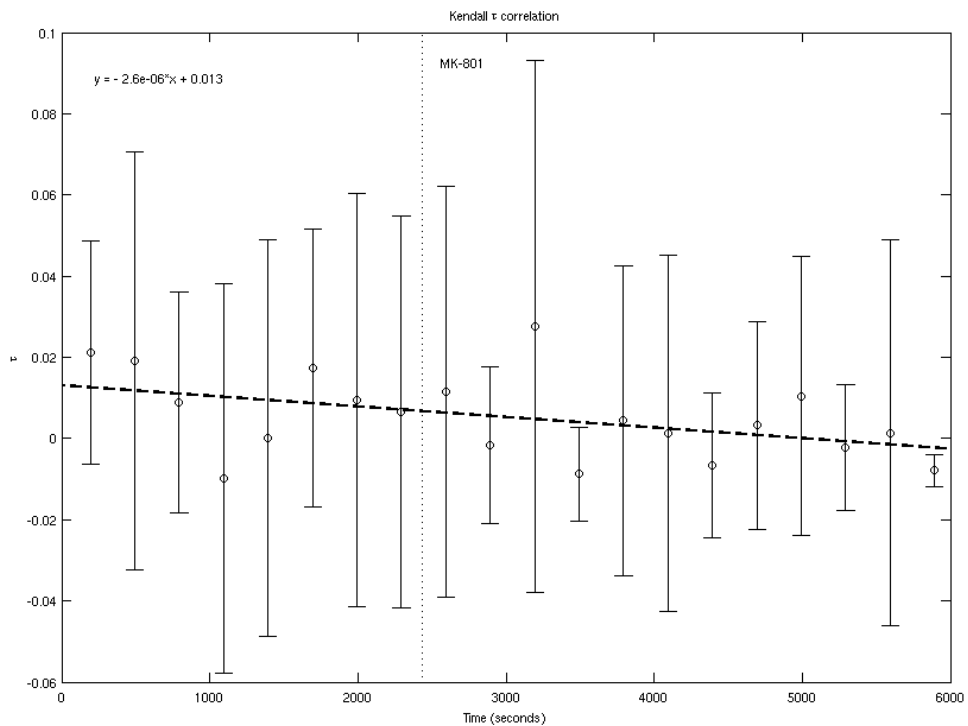

Figure 4.16: Kendall τ correlation of all clusters (means of all possible couples) from the manual clustering of operator A for subject 2.
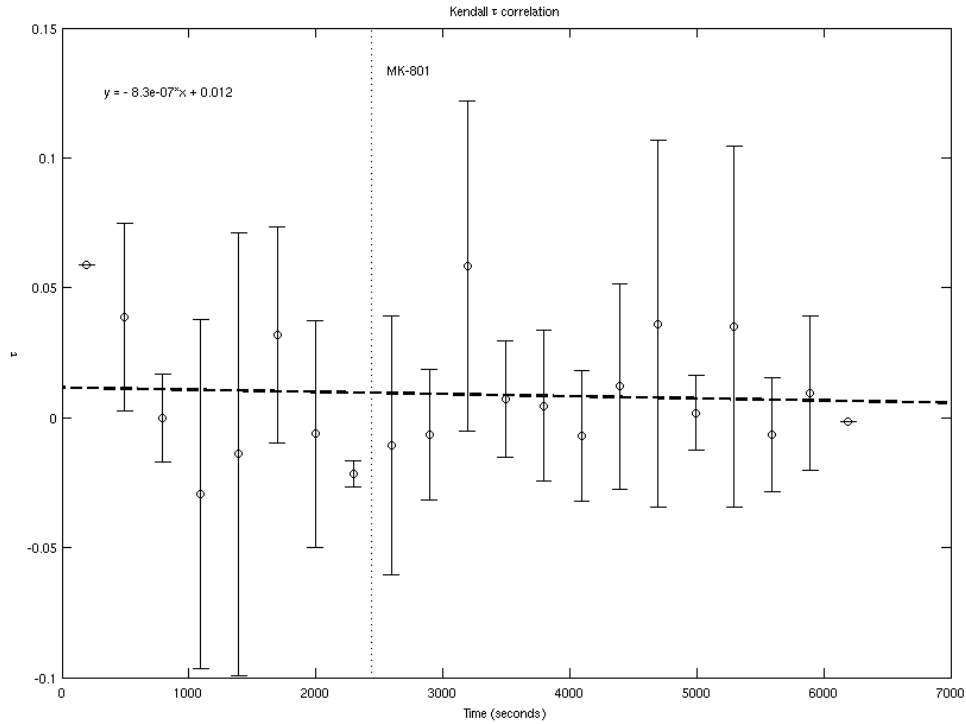
Figure 4.17: Kendall τ correlation of the good clusters (means of all possible couples) from the manual clustering of operator B for subject 2.
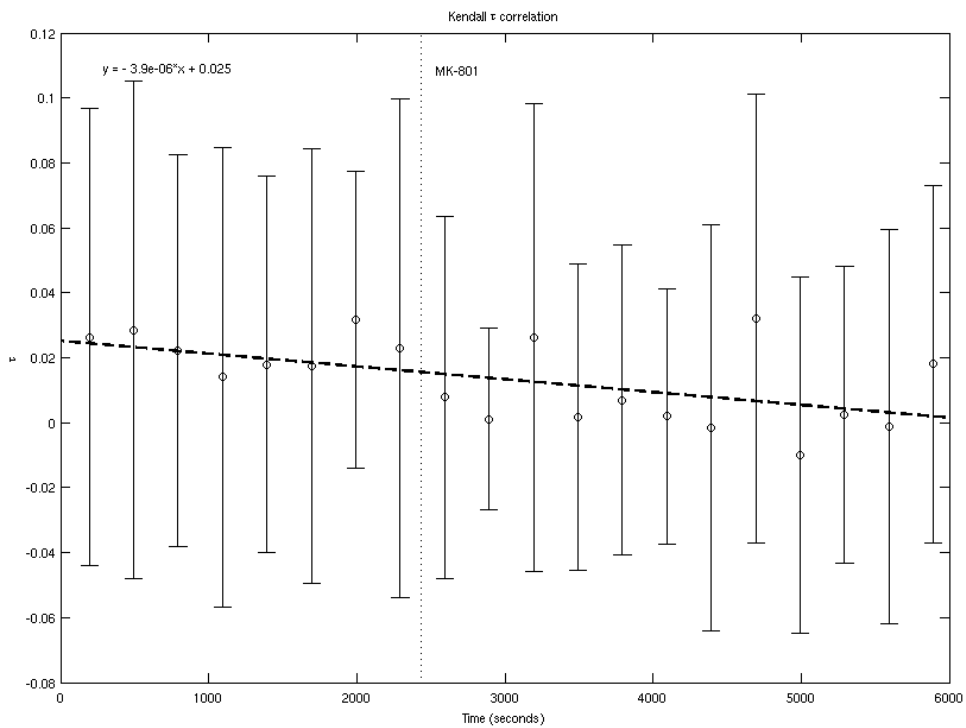

Figure 4.18: Kendall τ correlation of all clusters (means of all possible couples) from the manual clustering of operator B for subject 2.
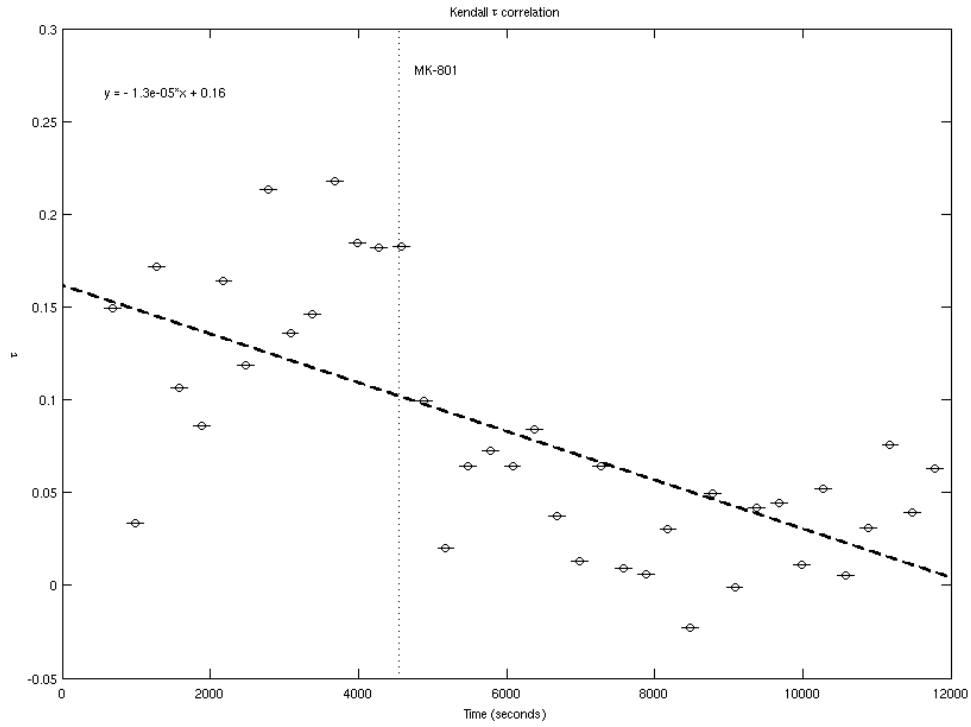
Figure 4.19: Kendall τ correlation of the good clusters (means of all possible couples) from the manual clustering of operator A for subject 3.
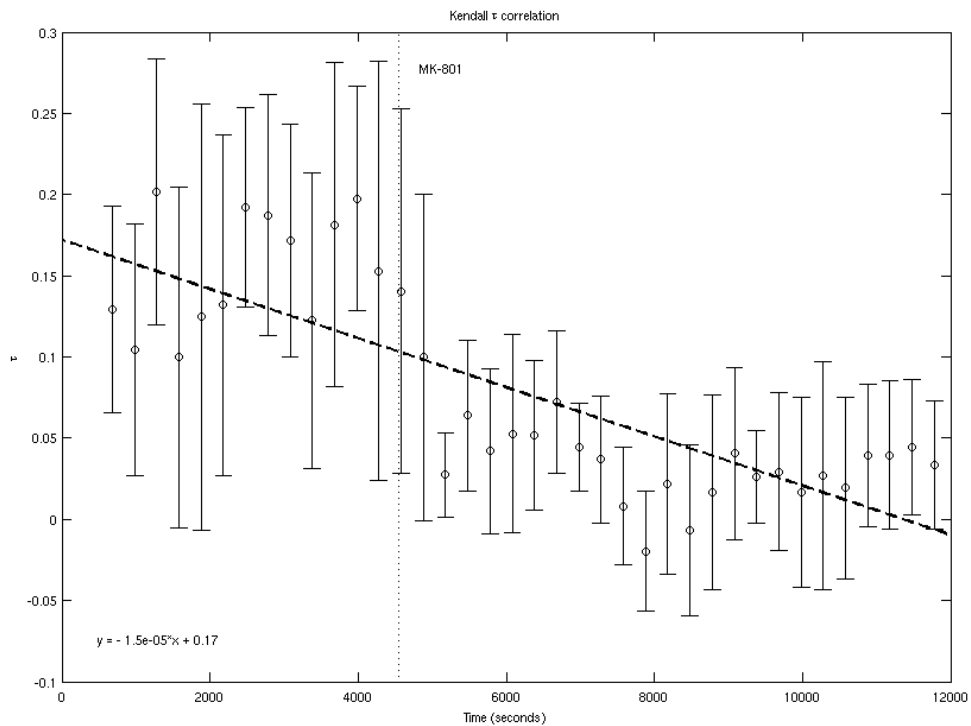

Figure 4.20: Kendall τ correlation of all clusters (means of all possible couples) from the manual clustering of operator A for subject 3.
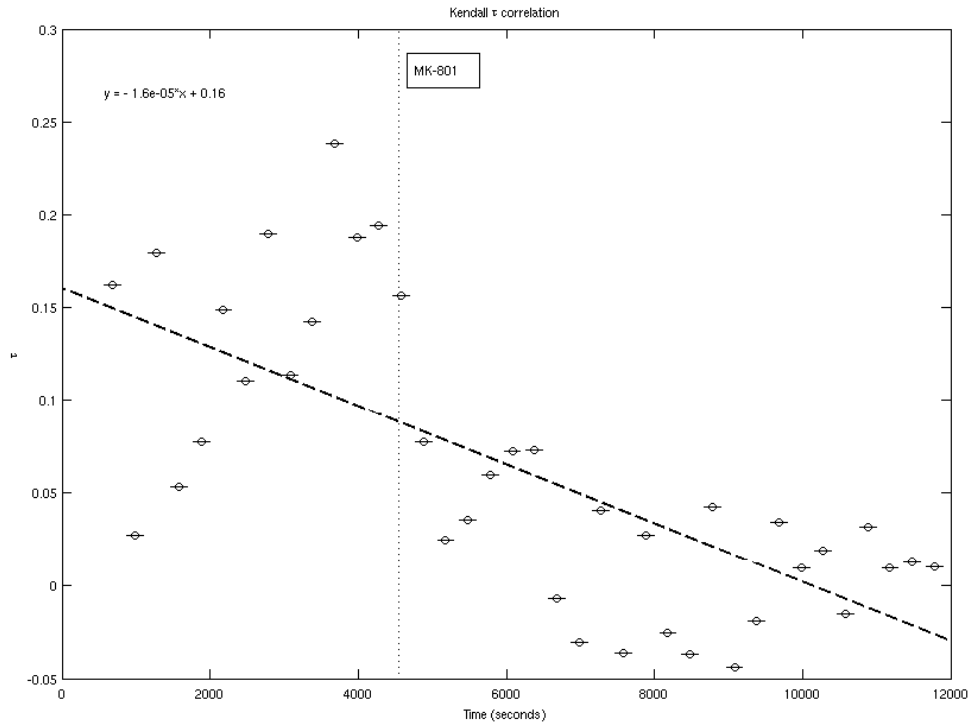
Figure 4.21: Kendall τ correlation of the good clusters (means of all possible couples) from the manual clustering of operator B for subject 3.
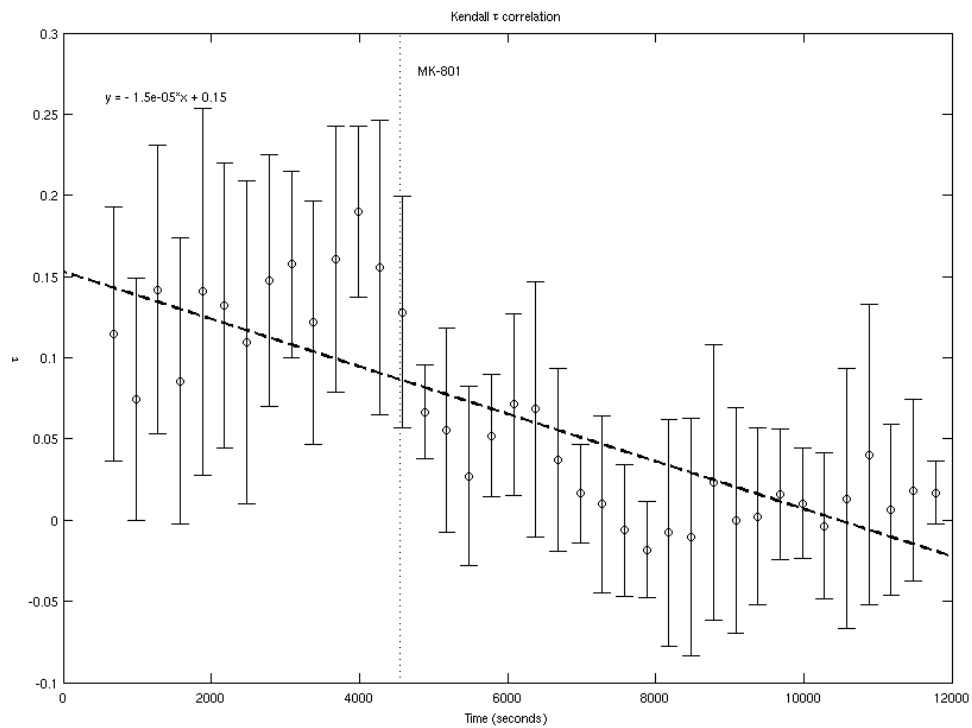

Figure 4.22: Kendall τ correlation of all clusters (means of all possible couples) from the manual clustering of operator B for subject 3.

Chapter 5

Discussion

The first aim of this thesis was to master the methods of extracellular unit recording and its subsequent analysis, especially cluster analysis. The cluster analysis was done using the MClust software. For this purpose it was neccessary to develop a software package that allowed to use the MClust software for our data and to evaluate the produced clusterings.

The second aim of this thesis was to study the effect of MK-801 on the hippocampal neuronal activity. To achieve this goal it was neccessary to learn how to make stable recordings lasting for several hours. So far I can present only preliminary data based on recordings in three subjects.

The long-term aim of my research is to study the unit activity in hippocampus in the MK-801 model of schizophrenia.

5.1 Recording of hippocampal neuronal activity in anaesthetized rats

The demonstrated comparison between automatic, semi-automatic and automatic clustering approaches shows that there is an apparent decrease of the average cluster quality in automatic clustering in comparison to the manual and semi-automatic.

In both recordings in subject 1 the total number of good clusters (the clusters with L-ratio < 0.1 and Isolation distance > 20) was highest for the automatic clustering. Nevertheless because the automatic algorithm clustered all the spikes including the apparent noise spikes, there has to be a following decision, which of the good spikes represent real neurons. This decision can be made according to the experience and according to the properties of spikes in the cluster (i.e. the average amplitude, signal energy or the waveform shape). Schmitzer-Torbert et al. (2005) suggest to test whether any reported results depend on the cluster quality in extracellularly recorded unit activity study and if so to exclude the poorly isolated neurons from further analysis.

Harris et al. (2000) reported that automatic clustering tools tend to overcluster the data (to produce more clusters than is the real number of recorded units). The data presented in this thesis are in agreement with this observation. The main problem of the automatic clustering is that it is not able to distinguish and eliminate spikes that are an apparent noise. The KlustaKwik program is also highly dependent on the parameters set, in both cases the total number of clusters was equal to the upper limit given to the program.

5.2 Effect of MK-801 on hippocampal neuronal activity in anaesthetized rats

Cognitive disorganization is thought to be the core deficit in the disorganized syndrome of schizophrenia (Phillips and Silverstein, 2003). It is characterized by hallucinations, disorganization, and thought disorder. This disorganization hypothesis is based on the observation that schizophrenic subjects are impaired at segregating relevant and irrelevant stimuli and selectively using associations between relevant cues (Olypher et al., 2006).

MK-801 has been used as a model of cognitive disorganization in the behavioral experiments (Carlsson and Carlsson, 1989; Vales et al., 2006; Stuchlik et al., 2009) and it is suggested as the animal model of schizophrenia (Nilsson et al., 2001; Rung et al., 2005). Administration of low doses of MK-801 is reported to cause hyperlocomotion.

There are other models of cognitive disorganization used. Some works (Olypher et al., 2006) used tetrodotoxine (TTX) and reported short increase of the unit activity in the uninjected hippocampus (about 15 minutes) and changes in correlation of activity after unilateral TTX injection. Wesierska et al. (2005) described effect of unilateral TTX injection in behavioral experiments. They reported that the TTX injection abolished the ability of rats to organize place-avoidance behavior specifically when distal room and local arena cues were continuously dissociated.

Other laboratories tested phencyclidine as the model of the cognitive disorganization, reporting a high increase of the unit activity and changes in mutual correlation of neuronal activity (unpublished data).

5.2.1 Electrical activity of the hippocampus

Overall activity

The overall activity of hippocampus in relation to the administration of MK-801 was evaluated only for two subjects and the results therefore have to be considered as preliminary. In both recordings the overall activity measured as the mean firing rate in 300 s time frames significantly rises. This is in contradict with the expected stability of hippocampal activity (Buzsaki et al., 2002). Buzsaki et al. (2002) report that in a long-term scale the firing rates of individual neurones are relatively constant in an unchanging environment. The observed rise gives a good chance that there will be an observed effect of the MK-801, but it has to be confirmed in the following experiments. Control experiments with

administration of saline without MK-801 have to follow to exclude the possibility that the observed results are caused by the long lasting anaesthesia.

The observed rise of the activity should not be related directly to the complete blockage of the NMDA-receptors by MK-801, because the administered dose was low. It is more probable that the partial blockage of the NMDA-receptor caused a change of the neuronal network state.

Unit activity

After the recorded data were clustered, effect of the administration of MK-801 on the firing rate in individual clusters was tested. The firing rate was calculated in 300 s time frames and the values before and after the administration were statistically compared using a Mann-Whitney U-test.

In all clusterings there were units that showed a rise in the activity, fall of the activity or their activity remained unchanged (see Table 4.15). The fractions of these units are affected by the total number of clusters produced by each clustering and by the quality of the produced clusters. In all clusterings there were identified 2 good clusters with a rise of activity and 1 cluster with a fall of activity. In this aspect the clusterings were equal. In all cases the significance and the direction of the change were the same for the matching clusters, showing that the results are not significantly dependent on the clustering used.

The effect of affection of the NMDA-receptors has been also described in Kentros et al. (1998), who reported that even during a total blockade of NMDA-receptors the creation of firing fields remained intact and only their stability decreased. Kimura and Pavlides (2000) reported experiments with potentiation of LTP in which the unit activity changed in both directions depending on the initial state of the unit. They suggest that changes in synaptic efficacy produce dynamic changes in cell activity.

Correlation

Testing of correlation between clusters tries to uncover possible changes of synchronicity of the neuronal network. Olypher et al. (2006) describes observed increase of correlation of previously weakly correlated units in response to the unilateral TTX injection, causing impairment of the selective activation and inhibition of stored spatial representations.

In the data recorded in subject 2 there is no apparent effect of administration of MK-801 on the correlation of firing between clusters. In the data recorded in

subject 3 there is an observed decrease of correlation in response to the administration of MK-801.

The results show that there is no difference between the correlation calculated from all clusters in comparison with the correlation calculated from the clusters with a good quality. There is also no difference between the results from independent operators. This gives a good chance that the results from this kind of experiments will be relatively immune to the clustering method used.

The real effect of MK-801 has to be widely examined in the following experiments to confirm or reject the preliminary data described in this thesis.

Chapter 6

Conclusion

Extracellular recordings of neuronal activity have an indispensable role in today's electrophysiology. As the technical equipment improves, the overall quality of recordings is rising. In past the classical single-neurone recording methods led to "neurone-centric" concepts of neural coding, whereas more recent multi-neurone population recordings have inspired "population-centric" concepts of distributed processing in neural systems. Dynamic fluctuations in neural population functions thus involve subtle changes in the overall pattern of neural activity. (Chapin, 2004)

This thesis focuses on the cluster analysis as the key tool for evaluation of extracellular recordings. The reported experiments show a small influence of chosen cluster analysis algorithms on the experimental results as well as a small influence of the cluster quality.

The effect of MK-801 is showed by means of the overall and unit activity and by changes of correlation between the units. The data show a possible rise of overall activity as well as changes of activity of individual neurones. The effect on neuronal network synchronicity showed a decrease of correlation in one recording. This observation has to be confirmed or rejected in the subsequent experiments.

The data have to be considered as preliminary and the research will be continued.

Bibliography

Aksenova, T. I. et al. (2003). An unsupervised automatic method for sorting neuronal spike waveforms in awake and freely moving animals. *Methods*, 30:178–187.

Alberts, B. et al. (2002). *Molecular Biology of The Cell*, chapter 11. Garland Science, 4th edition.

Andersen, P., Morris, R., Amaral, D., et al., editors (2007). *The hippocampus book*. Oxford University Press.

Blanche, T. J. and Swindale, N. V. (2006). Nyquist interpolation improves neuron yield in multiunit recordings. *Journal of Neuroscience Methods*, 155:81–91.

Bubenikova-Valesova, V., Horacek, J., Vrajova, M., and Hoschl, C. (2008). Models of schizophrenia in humans and animals based on inhibition of NMDA receptors. *Neuroscience & Biobehavioral Reviews*, 32(5):1014–1023.

Buzsaki, G. (1986). Hippocampal sharp waves: Their origin and significance. *Brain Research*, 398(2):242–252.

Buzsaki, G. (2002). Theta oscillations in the hippocampus. *Neuron*, 33:1–20.

Buzsaki, G. (2004). Large-scale recording of neuronal ensembles. *Nature Neuroscience*, 7:446–451.

Buzsaki, G., Csicsvari, J., Dragoi, G., Harris, K., Henze, D., and Hirase, H. (2002). Homeostatic maintenance of neuronal excitability by burst discharges in vivo. *Cerebral cortex*, 12(9):893.

Carlsson, M. and Carlsson, A. (1989). The NMDA antagonist MK-801 causes marked locomotor stimulation in monoamine-depleted mice. *Journal of neural transmission*, 75(3):221–226.

Celeux, G. and Govaert, G. (1992). A Classification EM algorithm for clustering and two stochastic versions. *Comput. Stat. Data Anal.*, 14(3):315–332.

Chapin, J. K. (2004). Using multi-neuron population recordings for neural prosthetics. *Nature Neuroscience*, 7:452–455.

Csicsvari, J., Henze, D. A., Jamieson, B., Harris, K. D., Sirota, A., Bartho, P., Wise, K. D., and Buzsaki, G. (2003). Massively parallel recording of unit and local field potentials with silicon-based electrodes. *Journal of Neurophysiology*, 90:1314–1323.

Daly, K. C., Wright, G. A., and Smith, B. H. (2004). Molecular features of odorants systematically influence slow temporal responses across clusters of coordinated antennal lobe units in the moth manduca sexta. *Journal of Neurophysiology*, 92:236–254.

Eichenbaum, H. and Otto, T. (1992). The hippocampus - what does it do? *Behavioral and Neural Biology*, 57:2–36.

Eyjolfsson, E., Brenner, E., Kondziella, D., and Sonnewald, U. (2006). Repeated injection of MK801: An animal model of schizophrenia? *Neurochemistry international*, 48(6-7):541–546.

Fix, J. D. (2008). *Neuroanatomy*, pages 266–268. Lippincott Williams and Wilkins.

Freund, T. and Buzsaki, G. (1996). Interneurons of the hippocampus. *Hippocampus*, 6(4):347–470.

Gold, C., Henze, D. A., Koch, C., and Buzsaki, G. (2006). On the origin of the extracellular action potential waveform: A modeling study. *Journal of Neurophysiology*, 95:3113–3128.

Green, K. F. and Rawlins, J. N. P. (1979). Hippocampal theta in rats under urethane: Generators and phase relations. *Electroencephalography and Clinical Neurophysiology*, 47:420–429.

Hara, K. and Harris, R. A. (2002). The anesthetic mechanism of urethane: The effects on neurotransmitter-gated ion channels. *Anesthetic Pharmacology*, 94:313–8.

Harris, K. D. (2002). KlustaKwik Automatic Cluster Analysis, version 1.8. http://klustakwik.sourceforge.net/.

Harris, K. D., Henze, D. A., Csicsvari, J., Hirase, H., and Buzsaki, G. (2000). Accuracy of tetrode spike separation as determined by simultaneous intracellular and extracellular measurements. *Journal of Neurophysiology*, 84:401–414.

Hazan, L., Zugaro, M., and Buzsaki, G. (2006). Klusters, NeuroScope, NDManager: A free software suite for neurophysiological data processing and visualization. *Journal of Neuroscience Methods*, 155:207–216.

Henze, D. A., Borhegyi, Z., Csicsvari, J., Mamiya, A., Harris, K. D., and Buzsaki, G. (2000). Intracellular features predicted by extracellular recordings in the hippocampus in vivo. *Journal of Neurophysiology*, 84:390–400.

Horton, P. M., Nicol, A. U., Kendrick, K. M., and Feng, J. F. (2007). Spike sorting based upon machine learning algorithms (SOMA). *Journal of Neuroscience Methods*, 160:52–68.

Joshua, M., Elias, S., Levine, O., and Bergman, H. (2007). Quantifying the isolation quality of extracellularly recorded action potentials. *Journal of Neuroscience Methods*, 163:267–282.

Kandel, E., Schwartz, J., Jessell, T., Mack, S., and Dodd, J. (1991). *Principles of neural science*. Elsevier New York.

Kentros, C., Hargreaves, E., Hawkins, R., Kandel, E., Shapiro, M., and Muller, R. (1998). Abolition of long-term stability of new hippocampal place cell maps by NMDA receptor blockade. *Science*, 280(5372):2121.

Kimura, A. and Pavlides, C. (2000). Long-term potentiation/depotentiation are accompanied by complex changes in spontaneous unit activity in the hippocampus. *Journal of Neurophysiology*, 84(4):1894.

Klement, D., Pastalkova, E., and Fenton, A. A. (2005). Tetrodotoxin infusions into the dorsal hippocampus block non-locomotor place recognition. *Hippocampus*, 15(4):460–471.

Kramis, R., Vanderwolf, C., and Bland, B. (1975). Two types of hippocampal rhytmical slow activity in both the rabbit and the rat: Relations to behavior and effects of atropine, diethyl ether, urethane and pentrobarbital. *Expl Neurol.*, 49:58–85.

Lewicki, M. S. (1998). A review of methods for spike sorting: the detection and classification of neural action potentials. *Network*, 9:R53–78.

McBain, C. and Fisahn, A. (2001). Interneurons unbound. *Nature Reviews Neuroscience*, 2(1):11–23.

McNaughton, B. L., O'Keefe, J., and Barnes, C. A. (1983). The stereotrode: a new technique for simultaneous isolation of several single units in the central nervous system from multiple unit records. *J Neurosci Methods*, 8(4):391–397.

Mercer, L., Remley, N., and Gilman, D. (1977). Effects of urethane on hippocampal unit activity in the rat. *Brain Research Bulletin*, 3:567–570.

Montgomery, S. M., Betancur, M. I., and Buzsaki, G. (2009). Behavior-dependent coordination of multiple theta dipoles in the hippocampus. *Journal of Neuroscience*, 29(5):1381–1394.

Morris, R., Garrud, P., Rawlins, J., and O'Keefe, J. (1982). Place navigation impaired in rats with hippocampal lesions. *Nature*, 297(5868):681–683.

Morris, R. G. M., Anderson, E., Lynch, G. S., and Baudry, M. (1986). Selective impairment of learning and blockade of long-term potentiation by an n-methyl-d-aspartate receptor antagonist, ap5. *Nature*, 319:774–776.

Muller, R. (1996). A quarter of a century of place cells. *Neuron*, 17:813–822.

Nilsson, M., Waters, S., Waters, N., Carlsson, A., and Carlsson, M. (2001). A behavioural pattern analysis of hypoglutamatergic mice–effects of four different antipsychotic agents. *Journal of Neural Transmission*, 108(10):1181–1196.

Nunez, P. N. and Srinivasan, R. (2006). *Electric Fields of the Brain: The neurophysics of EEG*, chapter 3–6. Oxford University Press.

O'Keefe, J. and Nadel, L. (1978). *The Hippocampus as a Cognitive Map*. Oxford University Press.

O'Keefe, J. and Recce, M. L. (1993). Phase relationship between hippocampal place units and the EEG theta rhytm. *Hippocampus*, 3(3):317–330.

Olypher, A., Klement, D., and Fenton, A. (2006). Cognitive disorganization in hippocampus: a physiological model of the disorganization in psychosis. *Journal of Neuroscience*, 26(1):158.

Phillips, W. and Silverstein, S. (2003). Convergence of biological and psychological perspectives on cognitive coordination in schizophrenia. *Behavioral and Brain Sciences*, 26(01):65–82.

Press, W., Flannery, B., Teukolsky, S., Vetterling, W., et al. (2007). *Numerical recipes*. Cambridge university press Cambridge.

Redish, A. D. et al. (2010). MClust Spike Sorting Toolbox, version 3.5. http://redishlab.neuroscience.umn.edu/MClust/MClust.html.

Rex, C. S., Colgin, L. L., Jia, Y., Casale, M., Yanagihara, T. K., et al. (2009). Origins of an intrinsic hippocampal EEG pattern. *PLoS ONE*, 4(11).

Rung, J., Carlsson, A., Rydén Markinhuhta, K., and Carlsson, M. (2005). (+)-MK-801 induced social withdrawal in rats; a model for negative symptoms of schizophrenia. *Progress in Neuro-Psychopharmacology and Biological Psychiatry*, 29(5):827–832.

Rutishauser, U., Schuman, E. M., and Mamelak, A. N. (2006). Online detection and sorting of extracellularly recorded action potentials in human medial temporal lobe recordings, in vivo. *Journal of Neuroscience Methods*, 154:204–224.

Schmitzer-Torbert, N., Jackson, J., Henze, D., Harris, K., and Redish, A. (2005). Quantitative measures of cluster quality for use in extracellular recordings. *Neuroscience*, 131:1–11.

Shepherd, G. (2004). *The synaptic organization of the brain*. Oxford University Press New York.

Sirota, A. and Buzsaki, G. (2005). Interaction between neocortical and hippocampal networks via slow oscillations. *Thalamus Relat Syst.*, 3(4):245–259.

Steele, R. J. and Morris, R. G. (1999). Delay-dependent impairment of a matching-to-place task with chronic and intrahippocampal infusion of the nmda-antagonist d-ap5. *Hippocampus*, 9(2):118–136.

Stuchlik, A., Petrasek, T., and Vales, K. (2009). Effect of alpha1-adrenergic antagonist prazosin on behavioral alterations induced by MK-801 in a spatial memory task in Long Evans rats. *Physiol. Res*, 58:733–740.

Takahashi, S., Anzai, Y., and Sakurai, Y. (2003). Automatic sorting for multi-neuronal activity recorded with tetrodes in the presence of overlapping spikes. *Journal of Neurophysiology*, 89:2245–2258.

Tan, P., Steinbach, M., and Kumar, V. (2005). *Introduction to Data Mining*, chapter 8. Addison Wesley.

Traub, R. D., Whittington, M. A., Colling, S. B., Buzsaki, G., and Jefferys, J. G. R. (1996). Analysis of gamma rhythms in the rat hippocampus in vitro and in vivo. *Journal of Physiology*, 493(2):471–484.

Vales, K., Bubenikova-Valesova, V., Klement, D., and Stuchlik, A. (2006). Analysis of sensitivity to MK-801 treatment in a novel active allothetic place avoidance task and in the working memory version of the Morris water maze reveals differences between Long-Evans and Wistar rats. *Neuroscience research*, 55(4):383–388.

Wesierska, M., Dockery, C., and Fenton, A. (2005). Beyond memory, navigation, and inhibition: behavioral evidence for hippocampus-dependent cognitive coordination in the rat. *Journal of Neuroscience*, 25(9):2413.

Wolansky, T., Clement, E. A., Peters, S. R., Palczak, M. A., and Dickson, C. T. (2006). Hippocampal slow oscillation: A novel EEG state and its coordination with ongoing neocortical activity. *Journal of Neuroscience*, 26(23):6213–6229.

List of Abbreviations

- **AcX** recording software

- **CA1**, **CA2**, **CA3**, **CA4** anatomical parts of Cornu Amonnis

- **CEM** classification expectation-maximization algorithm

- **DC** direct current

- **D.G.** dentate gyrus

- **EEG** electroencephalography

- **LIA** large irregular activity

- **LTP** long-term potentiation

- **MK-801** dizocilpine, non-competitive antagonist of NMDA receptors

- **NMDA** N-methyl-D-aspartate

- **PC** principal component or personal computer

- **PCA** principal component analysis

- **SNR** signal-to-noise ratio

- **TTX** tetrodotoxin